

Dynamical Seasonal Predictability of the Asian Summer Monsoon

K. R. SPERBER,* C. BRANKOVIC,⁺ M. DÉQUÉ,[#] C. S. FREDERIKSEN,[@] R. GRAHAM,[&] A. KITOH,**
C. KOBAYASHI,⁺⁺ T. PALMER,⁺ K. PURI,[@] W. TENNANT,^{##} AND E. VOLODIN^{@@}

*Program for Climate Model Diagnosis and Intercomparison, Lawrence Livermore National Laboratory, Livermore, California

⁺European Centre for Medium-Range Weather Forecasts, Reading, United Kingdom

[#]Centre National de Recherches Météorologiques, Toulouse, France

[@]Bureau of Meteorology Research Centre, Melbourne, Australia

[&]Met Office, Bracknell, Berkshire, United Kingdom

**Climate Research Department, Meteorological Research Institute, Japan Meteorological Agency, Tsukuba, Japan

⁺⁺Climate Prediction Division, Japan Meteorological Agency, Tokyo, Japan

^{##}South African Weather Bureau, Pretoria, South Africa

^{@@}Department of Numerical Mathematics, Moscow, Russia

(Manuscript received 5 July 2000, in final form 19 February 2001)

ABSTRACT

Ensembles of hindcasts from seven models are analyzed to evaluate dynamical seasonal predictability of 850-hPa wind and rainfall for the Asian summer monsoon (ASM) during 1987, 1988, and 1993. These integrations were performed using observed sea surface temperatures and from observed initial conditions. The experiments were designed by the Climate Variability and Predictability, Working Group on Seasonal to Interannual Prediction as part of the Seasonal Prediction Model Intercomparison Project. Integrations from the European Union Prediction of Climate Variations on Seasonal to Interannual Timescales experiment are also evaluated.

The National Centers for Environmental Prediction–National Center for Atmospheric Research and European Centre for Medium-Range Weather Forecasts reanalyses and observed pentad rainfall form the baseline against which the hindcasts are judged. Pattern correlations and root-mean-square differences indicate errors in the simulation of the time mean low-level flow and the rainfall exceed observational uncertainty. Most models simulate the subseasonal EOFs that are associated with the dominant variations of the 850-hPa flow during the ASM, but not with the fidelity exhibited by the reanalyses as determined using pattern correlations. Pattern correlations indicate that the first EOF, associated with the tropical convergence zone being located over the continental landmass, is best simulated. The higher-order EOFs are less well simulated, and errors in the magnitude and location of their associated precipitation anomalies compromise dynamical seasonal predictability and are related to errors of the mean state. In most instances the models fail to properly project the subseasonal EOFs/principal components onto the interannual variability with the result that hindcasts of the 850-hPa flow and rainfall are poor. In cases where the observed EOFs are known to be related to the boundary forcing, the failure of the models to properly project the EOFs onto the interannual variability indicates that the models are not setting up observed teleconnection patterns.

1. Introduction

The roots of contemporary seasonal forecasting of the boreal summer monsoon, in particular the Indian monsoon, date back to the late 1870s (Normand 1953). H. F. Blanford, the father of the All-India Meteorological Service, based his forecasts of Indian monsoon rainfall on preseason snowcover in the Himalayas (Blanford 1884). Presently, the role of Himalayan (and Eurasian) snowcover as a precursor to monsoon rainfall is still the subject of much debate and investigation (Barnett et al. 1989; Ferranti and Molteni 1999; Becker et al. 2001).

In the 1920s–1930s, Sir G. Walker imposed mathematical rigor to the forecast problem, introducing the use of the correlation coefficient to the meteorological community, with the goal of determining the conditions that “foreshadow” Indian summer monsoon rainfall (Walker and Bliss 1930). To this day, seasonal forecasts of summer monsoon rainfall are based primarily on statistical methods that take into account key indices associated with slowly varying components of the climate system, such as the El Niño–Southern Oscillation (ENSO; Krishna Kumar et al. 1995).

Dynamical seasonal predictability, if successful, would provide advantages over statistical methods, including (but not limited to) 1) a reliable estimate of the magnitude and regionality of the rainfall anomalies, 2) probabilistic forecasts of monsoon strength, and 3) an estimate of confidence bounds of the forecast based

Corresponding author address: Dr. Kenneth R. Sperber, Program for Climate Model Diagnosis and Intercomparison, Lawrence Livermore National Laboratory, P.O. Box 808, L-264, Livermore, CA 94550.

E-mail: sperber@space.llnl.gov

upon the spread of the ensemble members. However, dynamical seasonal predictability of the Asian summer monsoon (ASM) has remained elusive and as yet does not exceed that associated with statistical measures. This lack of predictability has been illustrated by integrations performed under the European Union Prediction of Climate Variations on Seasonal to Interannual Timescales (PROVOST) project (Brankovic and Palmer 2000). In this case, a contributing factor to the poor predictability was the magnitude of the systematic error of the seasonal mean monsoon, with the largest errors occurring in the vicinity of the tropical convergence zones (TCZ). These errors were of a magnitude comparable to the signal that was to be predicted. Furthermore, Sperber and Palmer (1996) have shown that the teleconnection between all-India rainfall and tropical sea surface temperature (SST) is not captured well by general circulation models (GCMs).

Predictability may also be limited by the influence of random subseasonal variations onto the seasonal mean. For example, Krishnamurti and Bhalme (1976), Sikka (1980), and Gadgil and Asha (1992) find that years of below-normal all-India rainfall (AIR) tend to be characterized by prolonged monsoon breaks with the TCZ preferentially located over the Indian Ocean. The degree to which the subseasonal variability is not predictable will have a direct impact on the accuracy of the hindcasts.

The main body of evidence supporting a link between subseasonal and interannual variability has been based upon model simulations (Fennessy and Shukla 1994; Ferranti et al. 1997), mainly through circumstantial evidence based upon the similarity of the spatial patterns of subseasonal and interannual variability. This led Palmer (1994) to propose a paradigm in which intra-seasonal variability is essentially chaotic, with the interannual variability being governed by the frequency of occurrence of the active (continental) versus the break (oceanic) phase. Consistent with the ideas of Charney and Shukla (1981), the suggestion is that the boundary forcing (e.g., SST) biases the system toward more active or break conditions.

Using the National Centers for Environmental Prediction–National Center for Atmospheric Research (NCEP–NCAR) reanalysis (Kalnay et al. 1996), Sperber et al. (1999, 2000a) investigated the link between subseasonal and interannual variability during the ASM for the period 1958–97. Using daily 850-hPa winds they identified sub-seasonal EOFs associated with the northward propagation of the TCZ, and a common pattern of variability that controlled the subseasonal and interannual variations of rainfall over India. Additionally, they clearly demonstrated that low-frequency variations of the basic state were responsible for systematically perturbing a subset of these EOFs/principal components (PCs), thus yielding the potential for probabilistic predictability of some aspects of the ASM.

The goals of this paper are to investigate ensembles

of hindcasts to determine the following: 1) Can GCMs accurately simulate the subseasonal EOFs that are associated with the dominant variations of the 850-hPa flow during the ASM? 2) Can the models represent the strong link between the 850-hPa flow and the rainfall observed on subseasonal timescales? 3) If so, are these EOFs/PCs correctly projected onto the seasonal mean monsoon to produce observed interannual variations of the 850-hPa flow and rainfall? 4) Is it possible to objectively discriminate among the ensemble members to ascertain which members are most reliable? Additionally, the results highlight the subseasonal patterns that are associated with errors in the mean states of the individual models.

The experimental design and the participating models are discussed in section 2. The time mean state is presented in section 3, and in section 4 the subseasonal variations are evaluated. In section 5 the projections of the subseasonal variations onto the interannual variability are presented, and discussion and conclusions are given in section 6.

2. The experimental design and the observed data

Recently, several efforts to assess dynamical seasonal predictability (DSP) have been undertaken. The most ambitious effort was the European Union PROVOST Project, which consisted of ensembles of integrations for each season for the period 1979–93. Only a limited number of modeling groups had the resources necessary to participate, and the project was European based. In an effort to assess DSP in a wider range of models, the Climate Variability and Predictability Numerical Experimentation Group-1 (now the Working Group on Seasonal to Interannual Prediction) initiated the Seasonal prediction Model Intercomparison Project (SMIP) at the suggestion of Dr. J. Shukla (Center for Ocean–Land–Atmosphere Studies). In all cases the models were forced with observed SSTs, and the initial conditions were taken from European Centre for Medium-Range Weather Forecasts (ECMWF) Reanalysis (in the case of PROVOST) or optionally NCEP–NCAR reanalysis in the case of SMIP.

The integrations analyzed in this paper are those that were contributed to the DSP archive at the Program for Climate Model Diagnosis and Intercomparison, and for which there were common years. Thus, we analyze summer monsoon hindcasts for 1987, 1988, and 1993. These years correspond to El Niño, La Niña, and near-normal conditions in the tropical Pacific Ocean, respectively. For these years we evaluate daily 850-hPa winds and rainfall for the period 1 June–30 September. Characteristics of the models analyzed are presented in Table 1. They span a wide range of horizontal and vertical resolutions, with the contribution from the South African Weather Bureau (SAWB) having the coarsest resolution, while the ECMWF model has the highest resolution. Further details of the models can be found in

TABLE 1. Model attributes.

Model	Resolution	Version	Ensemble size	References
BMRC (Australia) Bureau of Meteorology Research Centre	R31 L17	3.7	4	Hart et al. (1990) McAvaney and Colman (1993)
CNRM (France) Centre National de Recherches Météorologiques	T42 L31	Arpege/IFS Cycle 12	5	Déqué and Pielieuvre (1995)
DNM (Russia) Department of Numerical Mathematics	4° × 5° L21	A5421	4	Alekseev et al. (1999)
ECMWF (United Kingdom) European Centre for Medium Range Weather Forecasts	T63 L31	Cycle 13R4	9	Miller et al. (1995) Gibson et al. (1997)
JMA (Japan) Japan Meteorological Agency	T63 L30	GSM9603	4	JMA (1997)
SAWB (South Africa) South African Weather Bureau	T30 L18	COLA Version 1	4	Kirtman et al. (1997) Tennant (1999)
UKMO (United Kingdom) United Kingdom Meteorological Office	2.5° × 3.75° L19	HadAM2b	4	Hall et al. (1995) Graham et al. (2000)

the references given in Table 1. In the interest of brevity, the majority of results are presented from three of the seven participating models (ECMWF, JMA, and UKMO; see table for definition of acronyms) since they illustrate key aspects of the goals outlined in section 1. The conclusions based on this subset of models are equally applicable to the other four models (BMRC, CNRM, DNM, and SAWB). Results from all of the models are presented in Sperber et al. (2000b).

The daily 850-hPa wind from the NCEP–NCAR reanalysis is used to characterize the subseasonal and interannual variability over the ASM region. This reanalysis is a joint project between NCEP and NCAR to produce a multidecadal record of global atmospheric analyses with a data assimilation system that is unchanged (Kalnay et al. 1996). The data assimilation and forecast model are based on the global system that was implemented operationally at NCEP in January 1995. The model is run at a horizontal resolution of T62 and with 28 vertical levels. Moist convection is represented by a simplified Arakawa–Schubert parameterization

(Pan and Wu 1994) and clouds are diagnosed using a scheme based on Slingo (1987). The NCEP model uses a three-layer soil scheme based on that of Pan and Mahrt (1987) in which the temperature of the bottom layer is set to the annual mean climatological value. Data were assimilated using a spectral statistical interpolation/3D variational analysis method that requires no nonlinear normal-mode initialization. Monthly mean upper-air data on standard pressure surfaces have been supplied, already gridded onto a 2.5° latitude–longitude grid. Surface and 24-h forecast fields (e.g., precipitation) are given on the equivalent T62 Gaussian grid. The spinup of the hydrological cycle is small in the NCEP–NCAR reanalysis (e.g., Mo and Higgins 1996; Stendel and Arpe 1997).

To provide evidence of the robust nature of the subseasonal variations of the 850-hPa winds we have also analyzed the ECMWF reanalysis (ERA). A full description of the ERA is available in Gibson et al. (1996, 1997). It was performed using a special version of the ECMWF operational data assimilation system that includes a spectral T106 forecast model with 31 hybrid vertical levels and a fully three-dimensional semi-Lagrangian advection scheme. The forecast model is based on version 13r4 of the ECMWF Integrated Forecast System, which was operational between April 1995 and January 1996. The parameterization of moist processes uses the convective mass flux scheme of Tiedtke (1989) with prognostic clouds (Tiedtke 1993). The land surface scheme of Viterbo and Beljaars (1995) is based on a four-layer soil model and includes the effects of vegetation. A zero heat flux lower boundary condition is imposed and thus deep soil temperatures are not constrained to any climatology. Analyses were created every 6 h and a diabatic, nonlinear normal-mode initialization was applied. The 6-hourly T106 spectral upper-

TABLE 2. Pattern correlations and rmsd (m s^{-1}) of the time mean 850-hPa wind relative to NCEP–NCAR reanalysis for Jun–Sep 1987, 1988, and 1993 over the region 20°S–40°N, 60°–120°E. The statistics using ERA indicate the observational uncertainty. The data were re-gridded to the horizontal resolution of the NCEP–NCAR reanalysis prior to the analysis.

Model	Correlation	rmsd
ERA	0.96	1.24
ECMWF	0.91	1.84
JMA	0.85	2.74
UKMO	0.91	2.00
BMRC	0.89	3.23
CNRM	0.87	2.15
DNM	0.82	2.54
SAWB	0.81	2.90

TABLE 3. Pattern correlations and rmsd (mm day⁻¹) of the time mean precipitation relative to Xie and Arkin (1996) for Jun–Sep 1987, 1988, and 1993 over the region 21.25°S–41.25°N, 58.75°–121.25°E. The statistics using GPCP indicate the observational uncertainty. Comparisons with ECMWF and NCEP reanalyses are also included. The data were regridded to the horizontal resolution of the Xie–Arkin data prior to the analysis.

Model	Correlation	rmsd
GPCP	0.95	1.58
ERA	0.86	2.09
NCEP–NCAR	0.81	2.34
ECMWF	0.72	3.19
JMA	0.63	3.77
UKMO	0.77	2.66
BMRC	0.60	5.34
CNRM	0.75	2.81
DNM	0.58	4.43
SAWB	0.71	2.92

air data on model levels have been postprocessed to provide a range of variables on standard pressure levels on a 2.5° × 2.5° latitude–longitude grid.

The subseasonal variations of rainfall are determined using the Climate Prediction Center Merged Analysis of Precipitation (CMAP). This dataset uses essentially the same algorithm and data sources as the monthly CMAP dataset described by Xie and Arkin (1997). The version used is based on a blend of gauge data with satellite products, including Geostationary Operational Environmental Satellite Precipitation Index based on geostationary infrared data, Microwave Sounding Unit, (MSU), Outgoing Longwave Radiation-Based Precipitation Index, (OPI) Special Sensor Microwave/Imager (SSM/I) scattering and SSM/I emission. A detailed description of the pentad CMAP dataset is in preparation (P. Xie 1999, personal communication).

The observational uncertainty of the time mean rainfall is assessed by comparing the Xie and Arkin (1996) estimates with those from the Global Precipitation Climatology Project (GPCP; Huffman et al. 1995, 1997). This dataset is not totally independent of the Xie and Arkin (1996) rainfall as many of the same data sources are used, although GPCP does not use MSU or OPI data. However, the processing of the satellite data and the blending method with other data sources are different. Comparisons of the CMAP and GPCP data are given by Gruber et al. (2000) and Curtis et al. (2001, manuscript submitted to *J. Hydrometeor.*).

3. Time mean of the 850-hPa wind and rainfall

The lower-tropospheric Somali jet is one of the most dramatic elements of the Asian summer monsoon. Initially, it develops in response to the land–sea temperature contrast due to the seasonal change in solar heating. Subsequently, the latent heating associated with convection plays an increasingly important role in the maintenance of the Somali jet. Importantly, the 850-hPa flow captures important elements of the large-scale and

TABLE 4. Pattern correlations of the model EOFs relative to those from NCEP–NCAR reanalysis. The statistics using ERA indicate the observational uncertainty. Numbers within brackets are the EOF counterparts of those observed (e.g., for NDM, EOF-7 is the counterpart to observed EOF-1). DNM did not simulate a counterpart to observed EOF-2. The data were regridded to the horizontal resolution of the NCEP–NCAR reanalysis prior to the analysis.

Model	EOF-1	EOF-2	EOF-3
ERA	0.97	0.96	0.86
ECMWF	0.83	0.59	0.41*
JMA	0.87	0.69	0.80
UKMO	0.68	0.67	0.34* (6)
BMRC	0.55	–0.25* (3)	0.40 (2)
CNRM	0.81	0.68	0.55
DNM	0.34* (7)		0.39 (4)
SAWB	0.74	0.51	–0.08*

* Although other simulated EOFs had larger pattern correlations, these EOFs gave the most realistic representations of the key features of the observed EOFs (see section 4a for details).

regional-scale monsoon circulation on interannual and subseasonal timescales (Webster et al. 1998; Annamalai et al. 1999; Sperber et al. 2000a).

The time mean of the June–September (JJAS) 850-hPa wind from the NCEP–NCAR reanalysis and the models for 1987, 1988, and 1993 are given in Fig. 1. While this is a short record, the spatial pattern of the reanalysis climatology in Fig. 1a is robust with respect to its climatology for 1958–97 presented in Sperber et al. (2000a). However, in the more restricted record the flow over central India and the western Bay of Bengal is more zonal, and the monsoon circulation is weaker by 1–2 m s⁻¹ (not shown). This is consistent with the interdecadal variability of the monsoon circulation discussed in Sperber et al. (2000a). We have assessed the observational uncertainty by comparing the NCEP–NCAR and ERA reanalyses over the region 20°S–40°N, 60°–120°E. As seen in Table 2, the pattern correlation between the two reanalyses is 0.96 and the root-mean-square difference (rmsd) is 1.24 m s⁻¹. Consistent with Annamalai et al. (1999), substantial differences between the two reanalyses occur mainly over the ocean (not shown) where little data were available to constrain the reanalyses.

The time mean of the ensembles from each model show a wide variety of 850-hPa flow patterns. ECMWF (Fig. 1b) underestimates the strength of the Somali jet, especially over the Arabian Sea, while JMA (Fig. 1c) overestimates its strength. In UKMO (Fig. 1d) the jet is too strong over the Arabian Sea and too weak over eastern Asia. In JMA and UKMO the jet is too weak over northern India and the Bay of Bengal. As seen in Table 2, the models have smaller pattern correlations and larger rmsd relative to the observational uncertainty, indicating that substantial errors exist in the simulations of the low-level summer monsoon circulation.

The JJAS time mean precipitation for 1987, 1988, 1993 from Xie and Arkin (1996) and the models are presented in Fig. 2. The observed rainfall, Fig. 2a, is

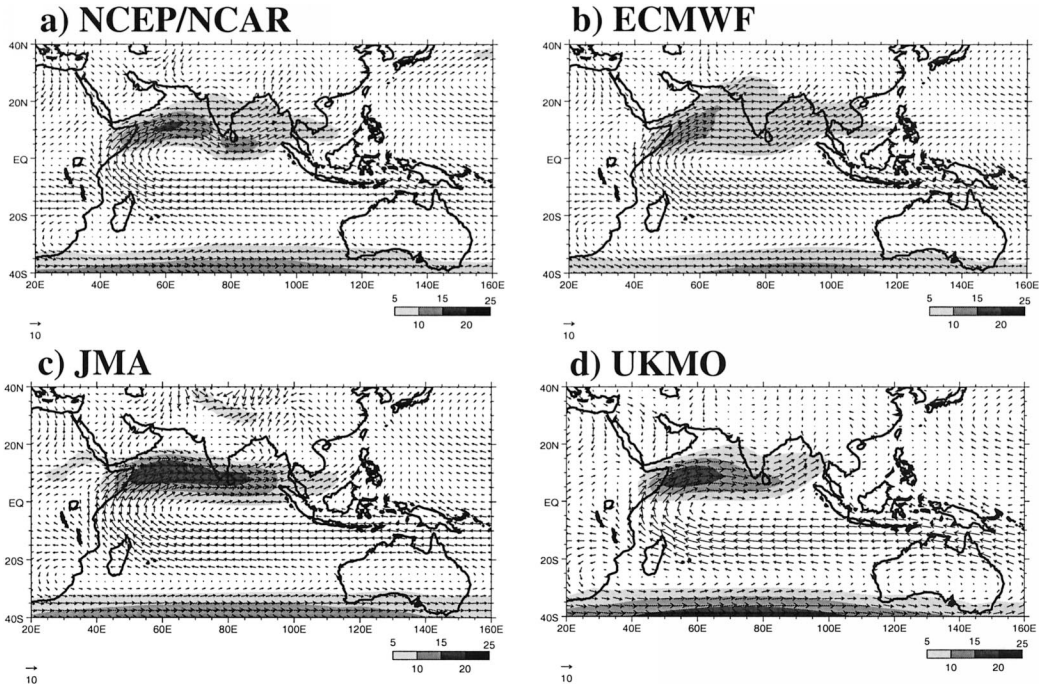


FIG. 1. Time mean 850-hPa wind for Jun–Sep 1987, 1988, and 1993. The zonal wind is shaded where it is $\geq 5 \text{ m s}^{-1}$. A unit vector corresponds to 10 m s^{-1} .

virtually identical to that for the period 1979–95 shown in Annamalai et al. (1999). As seen in Table 3, the Xie and Arkin (1996) and GPCP rainfall have a high pattern correlation (0.95). The rmsd of 1.58 mm day^{-1} is due

to lower rainfall values over the ocean in GPCP (not shown), where GPCP rainfall is approximately 15% below atoll gauge data (G. Huffman 2000, personal communication).

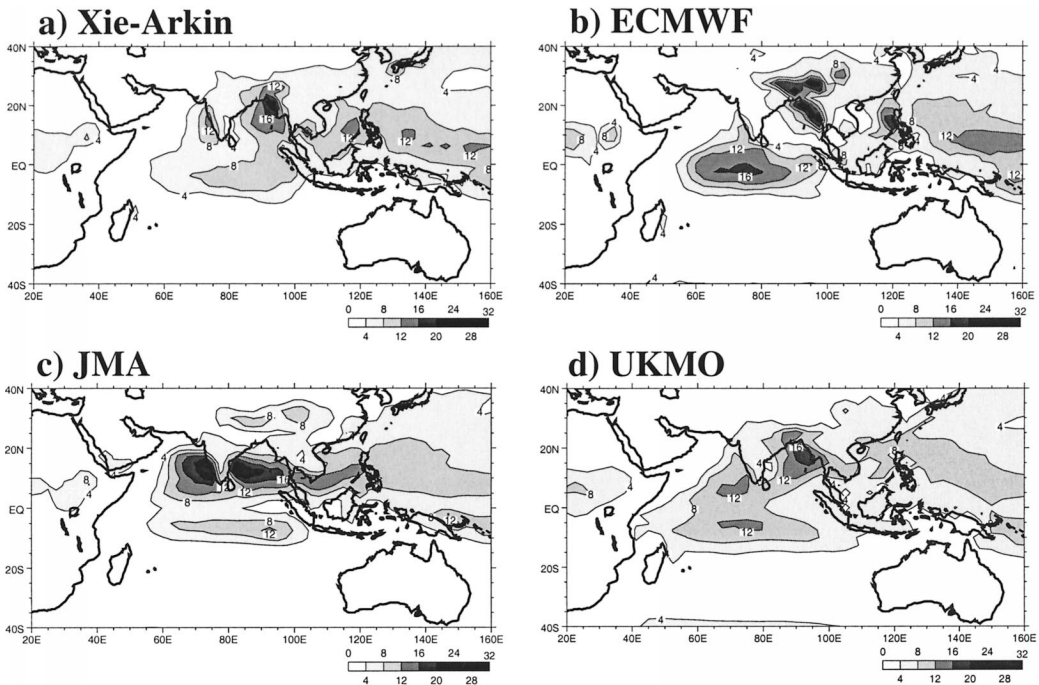


FIG. 2. Time mean rainfall for Jun–Sep 1987, 1988, and 1993. Contours and shading are plotted at 4, 8, 12, . . . mm day^{-1} .

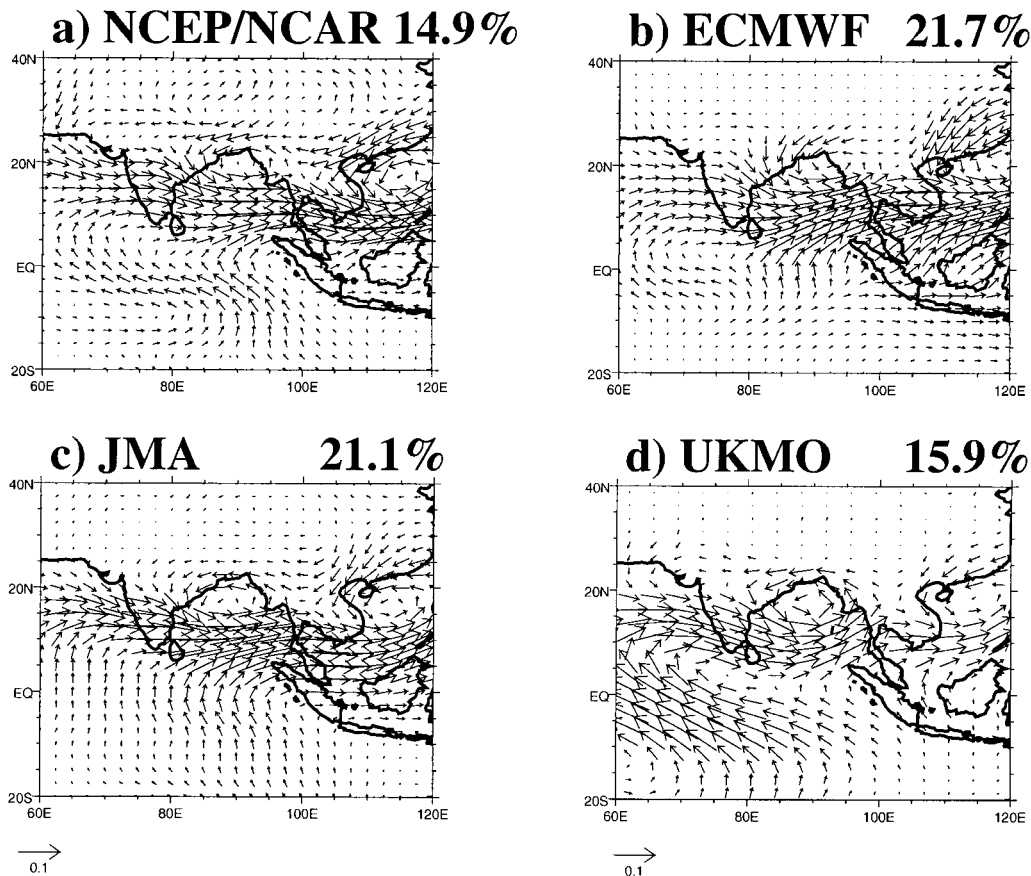


FIG. 3. EOF-1 of daily 850-hPa wind anomalies (calculated with respect to the climatological daily means) for Jun–Sep 1987, 1988, and 1993. The percentage variance explained is also given.

The errors in the simulated time mean rainfall are typically reflected as errors in the 850-hPa flow. This is consistent with the flow in the Tropics being governed mainly by diabatic heating. For ECMWF and UKMO (Figs. 2b and 2d) the enhanced rainfall along the west coast of India is poorly represented in association with the Somali jet being too weak and/or not extending far enough to the north. For the ECMWF model, the dry bias over India has been a pervasive problem, dating back to earlier versions of the model (Sperber et al. 1994). JMA (Fig. 2c) tends to overestimate the rainfall in the TCZ, and the rainfall at the head of the Bay of Bengal is underestimated in association with the poor representation of the low-level flow in that region (Fig. 1c). Table 3 indicates that the models have smaller pattern correlations and larger rmsd relative to the observational uncertainty, and they compare less favorably to the observations than either the NCEP–NCAR or ERA reanalyses.

For all models the 850-hPa wind and rainfall climatologies exceed the observational uncertainty. This suggests that some of the models may be of limited usefulness for seasonal predictability of the ASM. The degree to which this is the case, and the relationship

between errors in the climatologies and errors in the simulation of subseasonal variability will be explored next.

4. Subseasonal variability

a. EOF analysis of the 850-hPa flow

Subseasonal variability is characterized via EOF analysis of the 850-hPa winds, as performed in Sperber et al. (2000a). Prior to the analysis the climatological daily means (over all members of an individual model’s ensembles in the case of the hindcasts) have been removed at each grid point. EOF analysis of the NCEP–NCAR reanalyzed winds for 1987, 1988, and 1993 reveals that EOFs 1–3 (Figs. 3a, 4a, and 5a) are very robust, being virtually identical to their counterparts extracted from the 40 years examined by Sperber et al. (2000a). Additionally, these EOFs/PCs are consistent with those from ERA data for 1987, 1988, and 1993 (not shown). The pattern correlations with ERA for the respective EOFs are 0.97, 0.96, and 0.86 (Table 4), and the correlations with the PCs are 0.99, 0.95, and 0.88, respectively. These results attest to the robustness of these

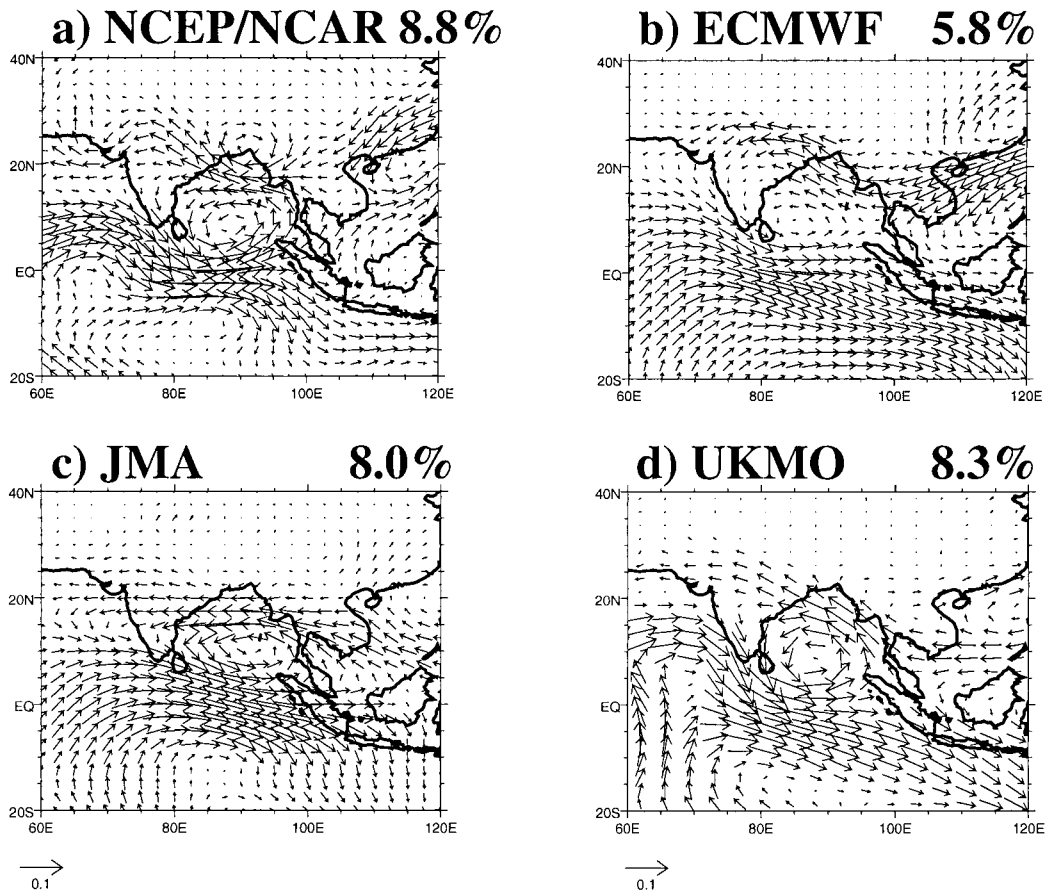


FIG. 4. As in Fig. 3 for EOF-2.

patterns for modulating subseasonal variability over the ASM region.

EOF-1 and EOF-2 are associated with the northward propagation of the TCZ, while EOF-3 is a common pattern of variability that is most important for controlling subseasonal and interannual variations of rainfall over India (Sperber et al. 2000a). These EOFs are consistent with composite differences of 850-hPa wind calculated with respect to subseasonal rainfall indexes of the tropical convergence zone (not shown) and all-India rainfall (AIR; Krishnamurthy and Shukla 2000). This indicates that the EOF analysis is extracting physically realistic patterns of variability over the chosen domain.

Given the robustness of the reanalyzed patterns we perform the EOF analysis separately for each model rather than performing a common principal component analysis of all models jointly. Additionally, a single analysis over all models would be a substantial compromise given the wide range of model performance in simulating the time mean rainfall and 850-hPa flow. Key features that should be represented by a model include the following: 1) For EOF-1 westerly anomalies located over the monsoon landmass (5°–20°N), and cyclonic circulation at the head of the Bay of Bengal, EOF-2

should have the same characteristics as EOF-1, but with the westerly anomalies located farther south (~0°–10°N) and with cyclonic anomalies over the Bay of Bengal. 2) For EOF-3 an anticyclonic–cyclonic couplet in the vicinity of India should be manifest.

Objective identification is performed by selecting the model EOF (of 10 retained in the analysis) that has the largest pattern correlation with that observed (Table 4; since an EOF/PC pair has an arbitrary sign convention, we have considered the reverse of those patterns that have negative pattern correlations). In a limited number of cases, when the pattern correlations are small (typically less than |0.5|), the EOF with the largest pattern correlation did not represent the key features outlined above. In these cases we have subjectively selected the model EOF that is most consistent with the aforementioned key aspects of the observed EOF.

As seen in Figs. 3b–d, ECMWF, JMA, and UKMO are realistic in their representation of EOF-1, particularly over the Asian continental latitudes. However, the pattern correlations in Table 4 indicate that the model EOFs have discrepancies that exceed the observational uncertainty. The main differences occur primarily over the western/central equatorial/southern Indian Ocean.

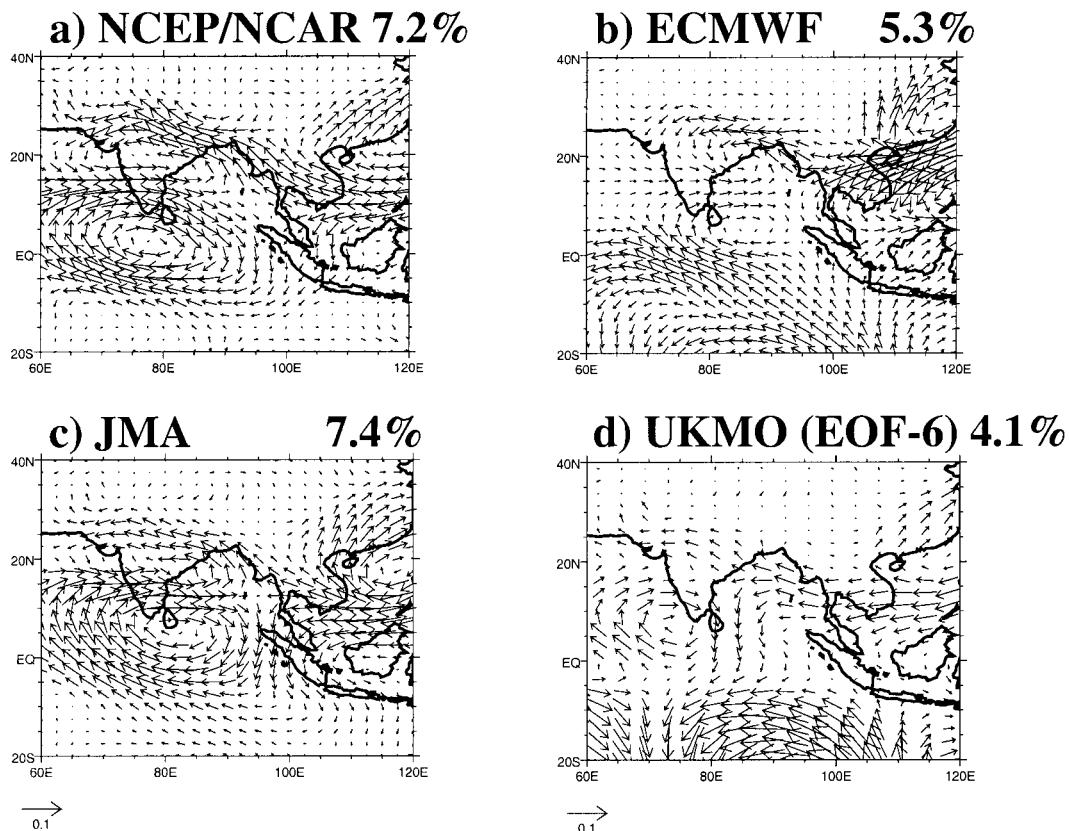


FIG. 5. As in Fig. 3 for EOF-3. For UKMO, EOF-6 is the counterpart to observed EOF-3.

For ECMWF and JMA, EOF-1 accounts for a larger fraction of the total variability than is observed.

EOF-2 (Fig. 4) is complementary to EOF-1, being associated with the initiation of the northward propagation of the TCZ (Sperber et al. 2000a). Relative to EOF-1 (Fig. 3a) the westerly anomalies are located south of the continental latitudes, and in the Bay of Bengal the cyclonic flow is also displaced farther south (Fig. 4a). Over the continental regions easterly anomalies are present. ECMWF, JMA, and UKMO (Figs. 4b–d) are realistic in their representation of these features, although discrepancies east of 100°E are apparent relative to the reanalysis. EOF 2 is relatively less well simulated than EOF-1 given its lower pattern correlations with the reanalysis.

EOF-3 (Fig. 5) is characterized by a cyclonic–anticyclonic pattern over and to the south of the Indian subcontinent. Over eastern Asia anticyclonic anomalies prevail, while to the south near the Maritime Continent the tendency is for cyclonic anomalies. JMA (Fig. 5c) is most adept at capturing this pattern, while ECMWF (Figs. 5b) exhibits an eastward displacement of the cyclone–anticyclone pair in the vicinity of India. With the exception of JMA, the models poorly represent the regionality of the flow south of the equator, and east of 100°E, and this is reflected in the pattern correlations in Table 4.

b. Relationship of the EOFs/PCs and rainfall

The rainfall anomalies associated with these EOFs are given in Figs. 6–8. These are composite differences of rainfall for \pm one standard deviation thresholds of the respective PCs. As seen in Fig. 6a, using the pentad CMAP rainfall, EOF-1/PC-1 is associated with a zonally oriented band of enhanced rainfall that extends from the Indian subcontinent to the western Pacific, with the largest loadings being located over the western Pacific. This is consistent with the 40-yr analysis in Sperber et al. (2000a). JMA and UKMO (Figs. 6c,d) represent well the rainfall anomalies associated with EOF-1/PC-1 (Figs. 3c,d). However, they tend to overestimate the amplitude of the anomalies over India and the Bay of Bengal. ECMWF (Fig. 6e) is similar, but it fails to capture the enhanced rainfall over western, central, and northeastern India seen in the CMAP composite (Fig. 6a). This is consistent with the pronounced dry bias in the time mean rainfall that this model exhibits over India (Fig. 2b).

The composite rainfall associated with EOF-2/PC-2 is given in Fig. 7. Relative to EOF-1, the positive rainfall anomalies (Fig. 7a) are typically weaker and displaced slightly southward, especially over the Bay of Bengal and southeast Asia. ECMWF and JMA (Figs. 7b,c) are most realistic in representing the rainfall anom-

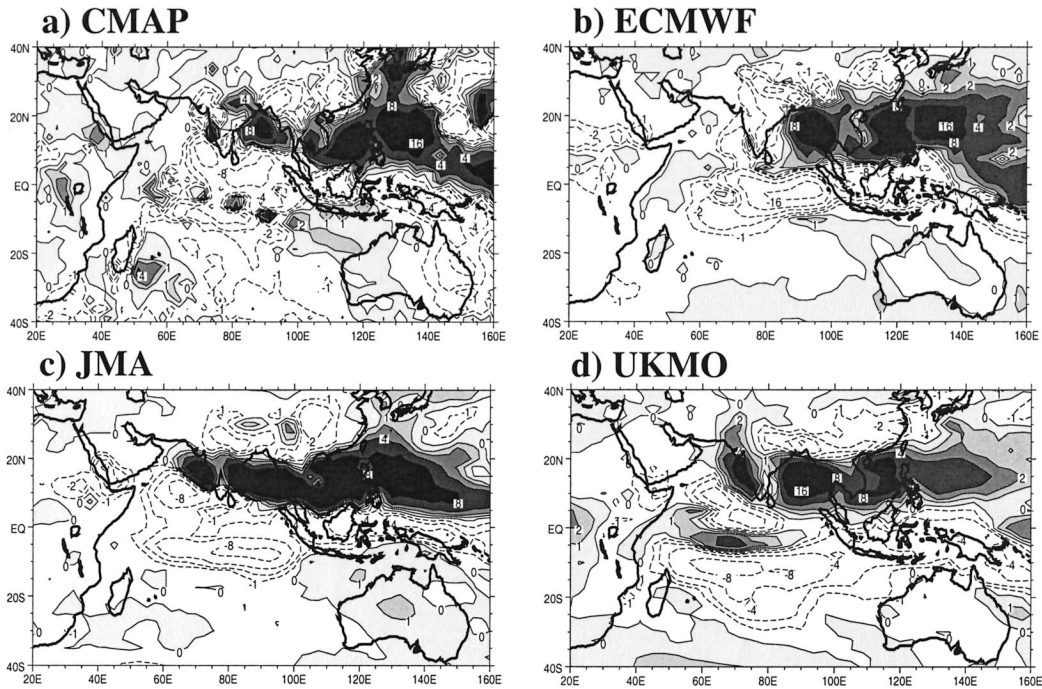


FIG. 6. Difference of daily composites of rainfall based on strong-weak days of the PC time series of EOF-1 using 1.0 and -1.0 standard deviation thresholds to define extreme days. The CMAP validation data is pentad based in which case the standardized daily PC time series was pentad averaged with extreme pentads defined using 1.0 and -1.0 standard deviation thresholds. Positive anomalies are shaded, and the contour interval is $\pm 0, 1, 2, 4, 8, \dots$ mm day $^{-1}$.

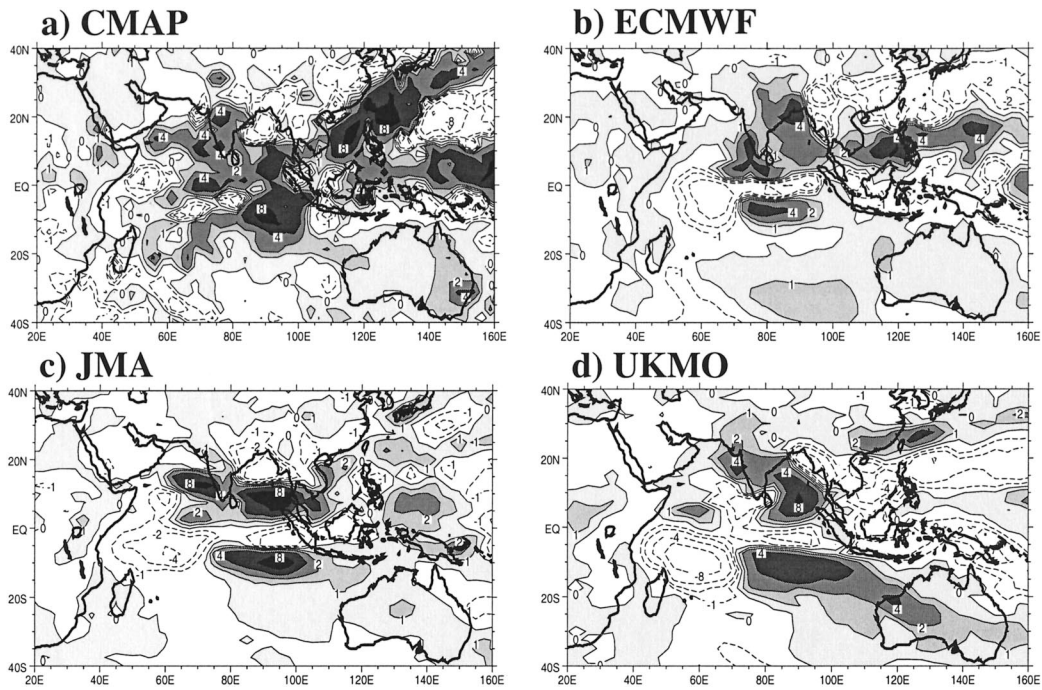


FIG. 7. As in Fig. 6 for EOF-2/PC-2.

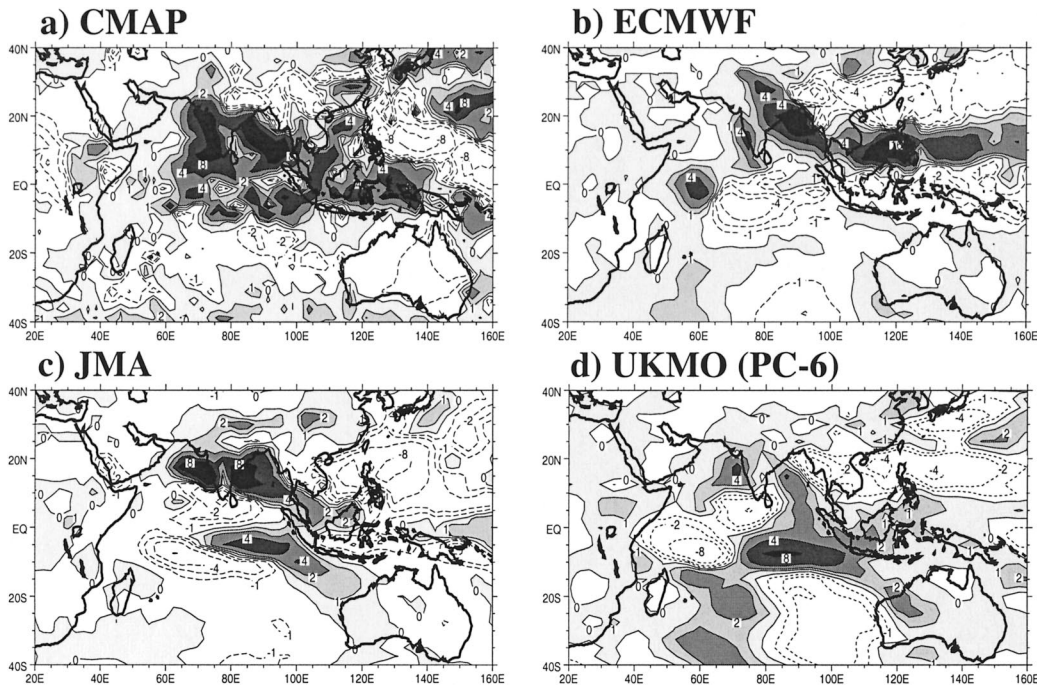


FIG. 8. As in Fig. 6 for EOF-3/PC-3.

alies. UKMO (Fig. 7d) performs best over India and the Bay of Bengal, but it fails to capture the extension of enhanced rainfall to the South China Sea, precisely where this model exhibited errors in EOF-2 (Fig. 4d).

For EOF-3/PC-3 the main signature in the observed rainfall is the southeastward tilt of enhanced rainfall that extends from India to the Maritime Continent (Fig. 8a). Over India the enhanced rainfall is associated with the cyclonic anomalies seen in Fig. 5a, while in the western Pacific (10°–25°N, 120°–140°E) and near the equator south of India the below-normal rainfall is associated with anticyclonic anomalies. The below-normal rainfall south of India is not as pronounced as from the longer record analyzed by Sperber et al. (2000a). ECMWF, JMA, and UKMO (Figs. 8c,d) are realistic in representing the pattern of rainfall anomalies in the vicinity of India. JMA and UKMO best represent the southeastward tilt of the rainfall into the western Pacific, but the anomalies are too weak, and the models incorrectly simulate below-normal rainfall over the South China Sea.

Considering all three EOFs, the models best represent the flow over India and the Bay of Bengal. They are most adept at simulating EOF-1 and its associated rainfall anomalies. For the higher-order EOFs regional differences relative to the observations become more manifest, with the most substantial errors occurring east of 100°E and south of the equator. Overall, the most realistic models are ECMWF, JMA, UKMO, and CNRM (Table 4). BMRC (not shown) exhibited a northward shift over the Indian longitudes. DNM (not shown) and SAWB (not shown), the coarse-resolution models, ex-

hibited difficulty in capturing the sharp gradients seen in the reanalysis.

While some of the models simulate the large-scale patterns of subseasonal rainfall anomalies, the regional differences relative to the observations indicate that accurate hindcasts of the magnitude and regionality of rainfall anomalies will be problematic. This is especially noticeable in the case of the rainfall associated with EOF-1/PC-1 for the ECMWF model (Fig. 6b), and the BMRC, DNM, and SAWB models (not shown). Their failure to capture the correct subseasonal rainfall signal over India has direct implications for forecasts/hindcasts of interannual variability. Even with a correct projection of EOF-1/PC-1 onto the seasonal mean rainfall, the rainfall over India due to this subseasonal pattern will be incorrect. The projections of the subseasonal modes onto the interannual variability are discussed in section 5.

5. Subseasonal and interannual variability

a. Systematic perturbations of the modes

Early work with a simple model to illustrate the paradigm of external forcing systematically perturbing chaotic variability (Palmer 1994), and a simple coupled model of summer monsoon (Webster et al. 1998), suggested that forced perturbations would be manifest as bimodality of the probability distribution function (PDF) of the principal component time series. Bimodality is an indication that the residence time in either state is longer than the time for the transition between the states. However, using 40 yr of NCEP–NCAR re-

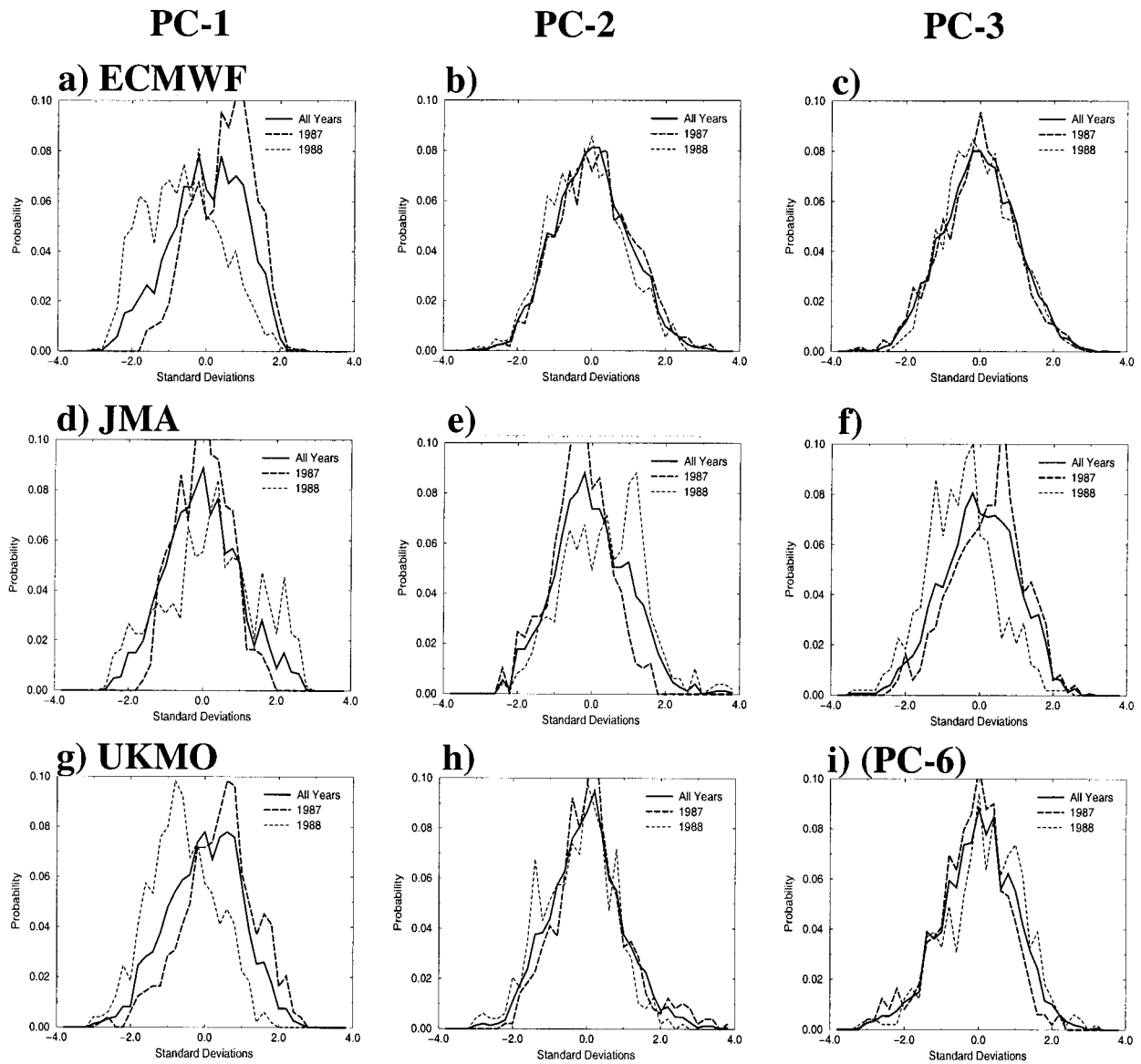


FIG. 9. PDFs of the simulated PC time series of EOFs 1–3 given in Figs. 3–5. Each of the PC time series were standardized prior to calculating the PDFs. The solid line is the PDF based on all years of data. The thick dashed line is the PDF for 1987, and the thin short-dashed line is the PDF for 1988.

analysis data, Sperber et al. (2000a) found that the perturbations of ASM subseasonal variability were manifested as changes in the means of Gaussian PDFs. If the models do not simulate Gaussian PDFs this will indicate that they are not capturing crucial characteristics of the temporal variability of the EOFs. Furthermore, predictability of the ASM has its inherent limitations since only a few of the observed patterns exhibit systematic perturbations.

As shown by Sperber et al. (2000a), EOF-1/PC-1 does not exhibit a systematic perturbation, varying randomly with respect to the phase of ENSO, strong versus weak year of AIR, strong versus weak years of the dynamical wind shear index (Webster and Yang 1992), and the

interdecadal variability of the land–sea temperature contrast over the monsoon region. This of course limits predictability of the ASM, since random perturbations of the dominant EOF will compromise DSP. EOF-2/PC-2 was systematically perturbed according to the phase of ENSO, with the mean of the PDF being negative during El Niño and positive during La Niña. However, 1988 was an exception with the projection being negative during 1988 attesting to the predictability being probabilistic rather than deterministic. EOF-3/PC-3 is systematically perturbed with respect to AIR, the mean of the PDF being positive (negative) during years of above-normal (below normal) AIR. That EOF-3/PC-3 is not systematically perturbed by ENSO is consistent

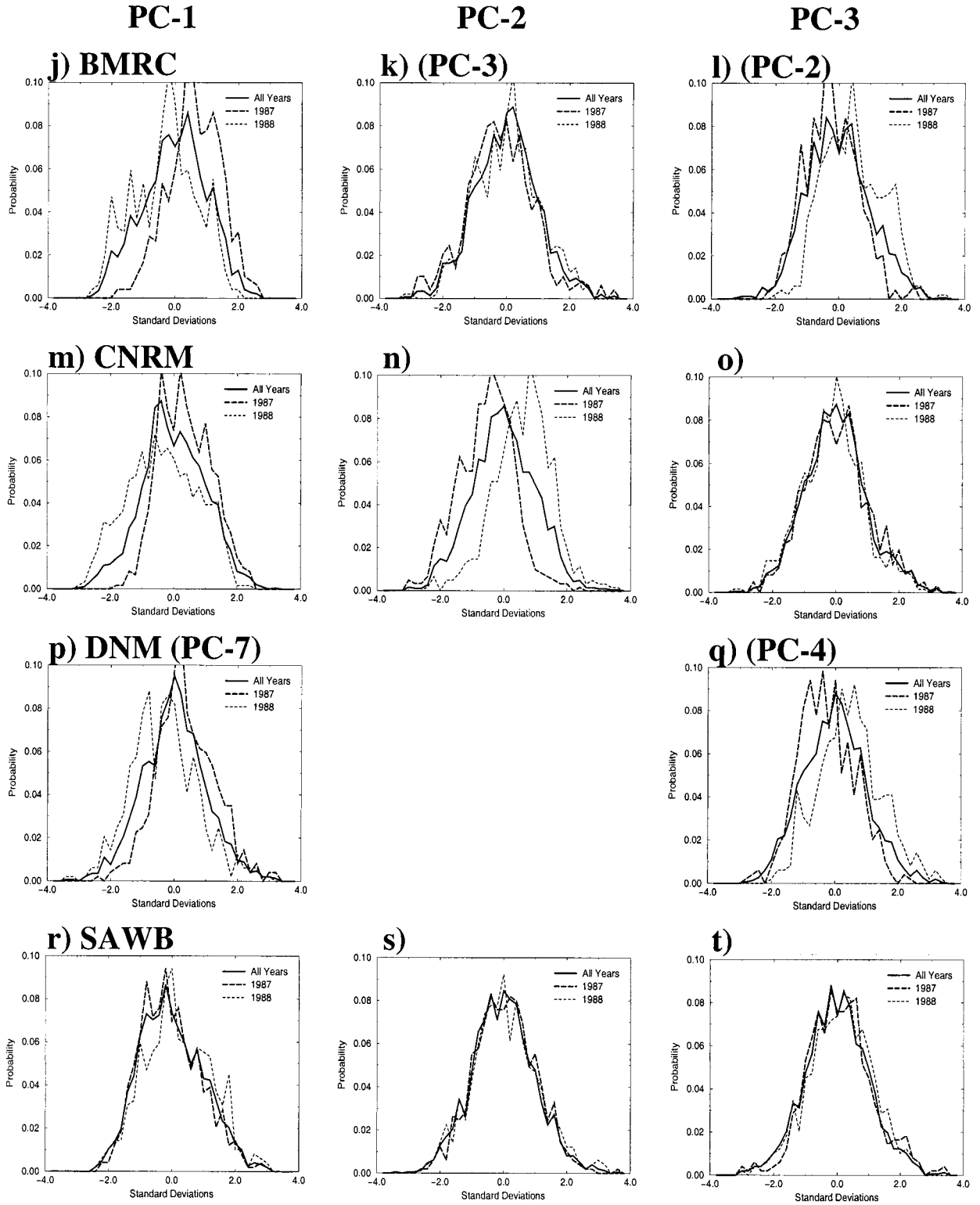


FIG. 9. (Continued)

with the lack of a unique relationship between Niño-3 SST and AIR over the period 1958–97, their correlation being -0.46 (Sperber et al. 2000a). If the models do not simulate PDFs that exhibit the observed systematic perturbations, this indicates that the models are not producing observed teleconnections to the boundary forcing, possibly related to shortcomings in model physics, thus further compromising DSP.

In Fig. 9 we show the PDFs of the PCs from the seven SMIP models to demonstrate their ability to simulate the aforementioned forced perturbations. The thick solid line is the PDF based on all ensemble members for 1987, 1988, and 1993. The shape of the PDFs is essentially Gaussian, in agreement with observations. Stratification is performed with respect to 1987 (thick long-dashed line) and 1988 (thin short-dashed line), corresponding to years of below-normal and above-normal AIR. Based upon the results of Sperber et al. (2000a), agreement with observations would result if the models exhibited a change in the mean of the PDF of PC-3 such that the mean is negative during 1987 and positive during 1988. Changes in the means of the PDFs are assessed as in Sperber et al. (2000a) by use of a two-tailed t -test that takes into account serial correlation. For PC-3 (from the reanalysis) JMA, UKMO (PC-6), BMRC (PC-2), and DNM (PC-4) (Figs. 9f, 9i, 9l, and 9q) exhibit systematic changes in the means of the PDFs at the 5% significance level. UKMO, BMRC, and DNM correctly simulate the observed perturbation, while in JMA the mean of the PDF is positive (negative) during 1987 (1988). Although this model gave an excellent representation of EOF-3 (Fig. 5f) and was able to establish the subseasonal link of EOF-3/PC-3 to rainfall (Fig. 8f), it does not properly project onto the interannual variability of the ASM.

Most models exhibit a demonstrative error by producing a significant perturbation to PC-1. This is contrary to the results of Sperber et al. (2000a), who found no perturbations of PC-1 as discussed above. ECMWF, UKMO, BMRC, CNRM, and DNM (PC-7) (Figs. 9a, 9g, 9j, 9m, and 9p) all indicate the mean of the PDF in 1987 to be greater than the mean of the PDF for 1988 at the 5% significance level. Thus, these models exhibit unrealistically robust perturbations to the TCZ due to the link of this EOF/PC to the subseasonal variation of rainfall (Fig. 6).

For EOF-2/PC-2, JMA and CNRM (Figs. 9e and 9n) the mean of the PDF is positive in 1988, contrary to the analysis by Sperber et al. (2000a, their Table 2). For these latter models the El Niño forcing in 1987 is consistent with the negative perturbation to PC-2 in Sperber et al. (2000a).

The results of the PDFs are encouraging in that they are basically Gaussian, consistent with reanalysis (Sperber et al. 2000a). Unfortunately, the simulated PDFs do not have the correct sensitivity to the boundary forcing on interannual timescales, indicating that predictability will typically be poor. The PDFs are, however,

TABLE 5. Seasonal means (Jun–Sep) of the PCs of the daily 850-hPa wind for 1987, 1988, and 1993 from reanalyses and the ECMWF ensembles. The dates indicate the start date of the integrations. The seasonal means of the PCs give the projection of each EOF onto the interannual variability. Bold indicates members that captured the correct sign of the observed projections for that year.

Year	Source	PC-1	PC-2	PC-3	
1987	NCEP	-2.5	-1.8	-14.3	
	ERA	-1.6	-2.4	-6.5	
	23 May ECMWF	26.3	7.5	-4.5	
	24 May ECMWF	25.6	3.8	-1.2	
	25 May ECMWF	17.5	-5.0	0.4	
	26 May ECMWF	27.8	3.0	3.5	
	27 May ECMWF	16.9	-3.2	-3.9	
	28 May ECMWF	4.5	-0.9	1.1	
	29 May ECMWF	40.2	5.2	-2.1	
	30 May ECMWF	0.7	3.1	-0.4	
	31 May ECMWF	24.9	5.1	-1.7	
	1988	NCEP	-7.6	-1.3	10.8
		ERA	-5.9	-1.4	5.3
23 May ECMWF		-26.5	9.0	13.1	
24 May ECMWF		-15.0	3.4	3.2	
25 May ECMWF		-37.2	-10.1	-5.8	
26 May ECMWF		-46.2	-1.5	-2.8	
27 May ECMWF		-56.0	-3.8	-2.2	
28 May ECMWF		-2.6	-5.2	5.5	
29 May ECMWF		6.3	-22.5	-12.6	
30 May ECMWF		-27.6	-1.1	2.8	
31 May ECMWF		-43.5	-1.3	0.9	
1993		NCEP	10.1	3.1	3.5
		ERA	7.5	3.7	1.2
	23 May ECMWF	18.7	2.1	3.4	
	24 May ECMWF	-9.3	-3.0	0.9	
	25 May ECMWF	3.6	0.6	3.9	
	26 May ECMWF	30.1	-8.7	-14.2	
	27 May ECMWF	-10.5	6.0	6.9	
	28 May ECMWF	-6.3	4.0	3.2	
	29 May ECMWF	7.7	1.7	1.1	
	30 May ECMWF	20.8	10.2	3.8	
	31 May ECMWF	9.4	1.5	-2.4	

based upon all members of the ensembles, and it possible that individual members may exhibit better agreement with observations.

As discussed in Sperber et al. (2000a), the seasonal averages of the PC time series give the projections of the subseasonal EOFs onto the interannual variability. The projections of the reanalyses and the ensemble members from each model are given in Tables 5–11. By comparing the NCEP–NCAR and ERA projections we have a measure of observational uncertainty. While the magnitudes of the loadings differ between the two reanalyses, for each summer and for each mode they both have the same sign. The observational uncertainty is typically smaller than the differences between ensemble members for any given model. This provides added support for our expectations with respect to how the models should project these EOFs/PCs onto interannual timescales.

Based on the findings of Sperber et al. (2000a), 1987 should be the most predictable via EOF-2 and EOF-3 due to the presence of El Niño forcing and below-normal

TABLE 6. As in Table 5 for JMA.

Year	Source	PC-1	PC-2	PC-3
1987	NCEP	-2.5	-1.8	-14.3
	ERA	-1.6	-2.4	-6.5
29 May	JMA	15.0	-8.1	15.8
30 May	JMA	14.7	-4.5	1.3
31 May	JMA	-3.7	-20.1	0.4
1 Jun	JMA	-23.6	-7.7	9.1
1988	NCEP	-7.6	-1.3	10.8
	ERA	-5.9	-1.4	5.3
29 May	JMA	49.9	15.6	-8.8
30 May	JMA	-40.6	2.1	-11.2
31 May	JMA	41.4	12.3	-24.2
1 Jun	JMA	-1.5	10.0	-18.9
1993	NCEP	10.1	3.1	3.5
	ERA	7.5	3.7	1.2
29 May	JMA	-28.5	2.3	15.4
30 May	JMA	-23.0	-8.8	2.0
31 May	JMA	-25.4	3.0	3.9
1 Jun	JMA	25.4	3.9	15.2

AIR. Then 1988 should exhibit predictability through EOF-3 due to above-normal AIR. In the next sections we evaluate the seasonal anomalies hindcast for the summer monsoons of 1987, 1988, and 1993.

b. 1987

Relative to the time mean of 1987, 1988, and 1993, the seasonal anomalies (June–September) of 850-hPa wind and the Xie and Arkin (1996) rainfall anomalies for 1987 are shown in Figs. 10a,b. Near India and the Bay of Bengal the anomalies are consistent with those presented in Sperber et al. (2000a) relative to the 1958–97 wind climatology and the 1979–95 rainfall clima-

TABLE 7. As in Table 5 for UKMO.

Year	Source	PC-1	PC-2	PC-3*
1987	NCEP	-2.5	-1.8	-14.3
	ERA	-1.6	-2.4	-6.5
28 May	UKMO	19.2	6.0	-7.5
29 May	UKMO	31.9	-5.7	-7.4
30 May	UKMO	-8.8	12.0	-3.4
31 May	UKMO	23.7	7.4	1.8
1988	NCEP	-7.6	-1.3	10.8
	ERA	-5.9	-1.4	5.3
28 May	UKMO	-26.1	-12.0	-0.5
29 May	UKMO	-32.8	0.5	12.5
30 May	UKMO	-27.2	-13.8	-1.4
31 May	UKMO	-18.2	-4.7	4.0
1993	NCEP	10.1	3.1	3.5
	ERA	7.5	3.7	1.2
28 May	UKMO	17.7	14.5	-3.3
29 May	UKMO	-11.8	-9.3	-2.0
30 May	UKMO	8.8	3.1	7.9
31 May	UKMO	23.7	1.9	-0.7

* PC-6 from UKMO.

TABLE 8. As in Table 5 for BMRC.

Year	Source	PC-1	PC-2*	PC-3**
1987	NCEP	-2.5	-1.8	-14.3
	ERA	-1.6	-2.4	-6.5
29 May	BMRC	13.7	-8.8	-11.7
30 May	BMRC	32.8	-5.6	-7.0
31 May	BMRC	12.3	-5.0	-6.4
1 Jun	BMRC	32.2	-0.4	-5.0
1988	NCEP	-7.6	-1.3	10.8
	ERA	-5.9	-1.4	5.3
29 May	BMRC	-28.5	4.1	10.1
30 May	BMRC	-5.6	3.7	15.9
31 May	BMRC	-25.9	-6.0	15.6
1 Jun	BMRC	15.3	2.2	15.3
1993	NCEP	10.1	3.1	3.5
	ERA	7.5	3.7	1.2
29 May	BMRC	6.9	6.1	-10.4
30 May	BMRC	-35.2	2.6	-13.7
31 May	BMRC	-9.1	7.8	-10.6
1 Jun	BMRC	-8.8	-0.9	8.0

* PC-3 from BMRC.
** PC-2 from BMRC.

tology. The anticyclonic anomalies over India are consistent with the negative projection of PC-3 in the re-analyses (Table 5) and thus the negative rainfall anomalies over the Indian subcontinent. The negative projection of PC-2, related to El Niño forcing, further enhances the northwesterly anomalies over northeast India. Negative projections of PCs-1–2 are also associated with below-normal rainfall over India (the reverse of Figs. 6a and 7a). As discussed in Sperber et al. (2000a), 1987 was an interesting year with the seasonal means of PCs 1–3 all being negative, such that constructive

TABLE 9. As in Table 5 for CNRM.

Year	Source	PC-1	PC-2	PC-3
1987	NCEP	-2.5	-1.8	-14.3
	ERA	-1.6	-2.4	-6.5
28 May	CNRM	9.0	-20.9	-2.9
29 May	CNRM	11.4	-18.1	3.9
30 May	CNRM	7.6	-10.0	4.1
31 May	CNRM	32.1	-14.5	1.9
1 Jun	CNRM	7.0	-21.6	-1.0
1988	NCEP	-7.6	-1.3	10.8
	ERA	-5.9	-1.4	5.3
28 May	CNRM	-25.5	11.5	-6.6
29 May	CNRM	-14.3	30.8	-2.8
30 May	CNRM	-25.6	26.2	-3.7
31 May	CNRM	-21.6	23.6	-0.9
1 Jun	CNRM	24.4	2.3	1.0
1993	NCEP	10.1	3.1	3.5
	ERA	7.5	3.7	1.2
28 May	CNRM	-11.3	-3.6	2.3
29 May	CNRM	8.6	3.5	-3.5
30 May	CNRM	-10.5	0.8	1.6
31 May	CNRM	10.5	-2.6	5.2
1 Jun	CNRM	-1.8	-7.4	1.6

TABLE 10. As in Table 5 for DNM. DNM did not simulate a counterpart to observed EOF-2.

Year	Source	PC-1*	PC-3**
1987	NCEP	-2.5	-14.3
	ERA	-1.6	-6.5
29 May	DNM	0.9	-3.0
30 May	DNM	4.2	0.1
31 May	DNM	0.0	-3.5
1 Jun	DNM	2.8	-1.2
1988	NCEP	-7.6	10.8
	ERA	-5.9	5.3
29 May	DNM	-1.2	3.8
30 May	DNM	-2.3	3.9
31 May	DNM	-0.9	2.6
1 Jun	DNM	-2.5	3.4
1993	NCEP	10.1	3.5
	ERA	7.5	1.2
29 May	DNM	0.0	-1.4
30 May	DNM	1.1	-0.9
31 May	DNM	-14	-3.5
1 Jun	DNM	-0.7	0.3

* PC-7 from DNM.

** PC-4 from DNM.

interference of these patterns gave rise to one of the strongest droughts of AIR. The enhanced rainfall near Burma (Fig. 10b) is associated with onshore flow from the northern Bay of Bengal, while in the near-equatorial Indian Ocean (80°–100°E) the enhanced rainfall is associated with convergent flow south and east of the cyclonic anomalies (Fig. 10a).

To date, seasonal anomalies from simulations have been directly compared to those from observations. Regions of agreement and disagreement are discussed, but the phenomena contributing to the regionality are not typically explored. Our approach here is to interpret the anomalies with respect to the projections of the sub-seasonal EOFs to ascertain if they arise due to the correct interrelationships of the EOFs/PCs.

For the ECMWF model, the enhanced rainfall near Burma (Fig. 10d) is similar to observations, as is the limited area of below-normal rainfall over southern India. However, particularly over India, the low-level wind anomalies (Fig. 10c) are not correctly simulated relative to observations (Fig. 10a). Rather, Table 5 indicates the presence of strong positive loadings of PC-1 in 1987 in all but two members of the ensemble. These positive loadings are reflected in the close correspondence of the total seasonal anomaly of 850-hPa wind (Fig. 10c) with EOF-1 (Fig. 3b) and the positive PDF perturbation seen in Fig. 9a. Thus, this EOF contributes (incorrectly) to the negative rainfall anomalies over India due to the incorrect composite difference of rainfall over India seen in Fig. 6b. The positive loadings of PC-1 are also associated with the enhanced rainfall at the head of the Bay of Bengal and the simulated cyclonic flow there, which in observations is predominantly due to the negative projection of PC-2.

TABLE 11. As in Table 5 for SAWB.

Year	Source	PC-1	PC-2	PC-3
1987	NCEP	-2.5	-1.8	-14.3
	ERA	-1.6	-2.4	-6.5
29 May	SAWB	-8.0	-1.2	2.5
30 May	SAWB	6.3	9.6	6.4
31 May	SAWB	0.7	5.1	3.7
1 Jun	SAWB	-3.1	3.9	8.3
1988	NCEP	-7.6	-1.3	10.8
	ERA	-5.9	-1.4	5.3
29 May	SAWB	-1.5	-2.6	1.0
30 May	SAWB	-3.1	-0.6	-2.7
31 May	SAWB	-1.2	-3.4	-2.7
1 Jun	SAWB	-2.3	-4.8	-2.2
1993	NCEP	10.1	3.1	3.5
	ERA	7.5	3.7	1.2
29 May	SAWB	2.3	-3.7	-2.8
30 May	SAWB	5.4	1.2	-1.6
31 May	SAWB	0.9	-2.0	-4.3
1 Jun	SAWB	3.7	-1.7	-5.7

For JMA, Table 6 indicates that negative loadings of PC-2 contribute to the enhanced rainfall over the northern Bay of Bengal (Fig. 10f), as do the overall positive loading (average over all ensemble members in 1987) of PC-1 and the incorrect positive loading of PC-3 (also noted in Fig. 9f). The errors in the projection of PC-1 and PC-3 also contribute to the incorrectly simulated enhanced rainfall over the continental regime and the incorrect low-level wind anomalies (Fig. 10e).

As with ECMWF, the incorrect strong positive projection of PC-1 from UKMO dominates (Table 7 and Fig. 9g), with the seasonal anomalies of 850-hPa wind and rainfall (Figs. 10g,h) essentially corresponding to EOF-1 (Fig. 3b) and its associated composite difference of rainfall (Fig. 6d). Incorrectly simulated positive loadings of PC-2 and PC-3 also contribute to the failure of the model of capture the low-level wind and rainfall anomalies in 1987.

c. 1988

The 850-hPa wind and rainfall anomalies for 1988, given in Figs. 11a,b, are mostly consistent with those relative to the longer record analyzed in Sperber et al. (1999). The exception is over the Arabian Sea, where in the longer record the wind anomalies are easterly adjacent to the west coast of India, with below-normal rainfall west of the southern tip of India. This is due to the difference in the time mean state relative to the longer climatologies used in Sperber et al. (1999, 2000a). Even so, the comparison here is consistent since the same years are used for calculating the reference time mean state for the models and observations. The spatial pattern of wind anomalies is nearly the opposite of that in 1987, consistent with the change in sign of the projection of PC-3 onto the seasonal anomaly (Table 5). With disturbances along the monsoon trough, cy-

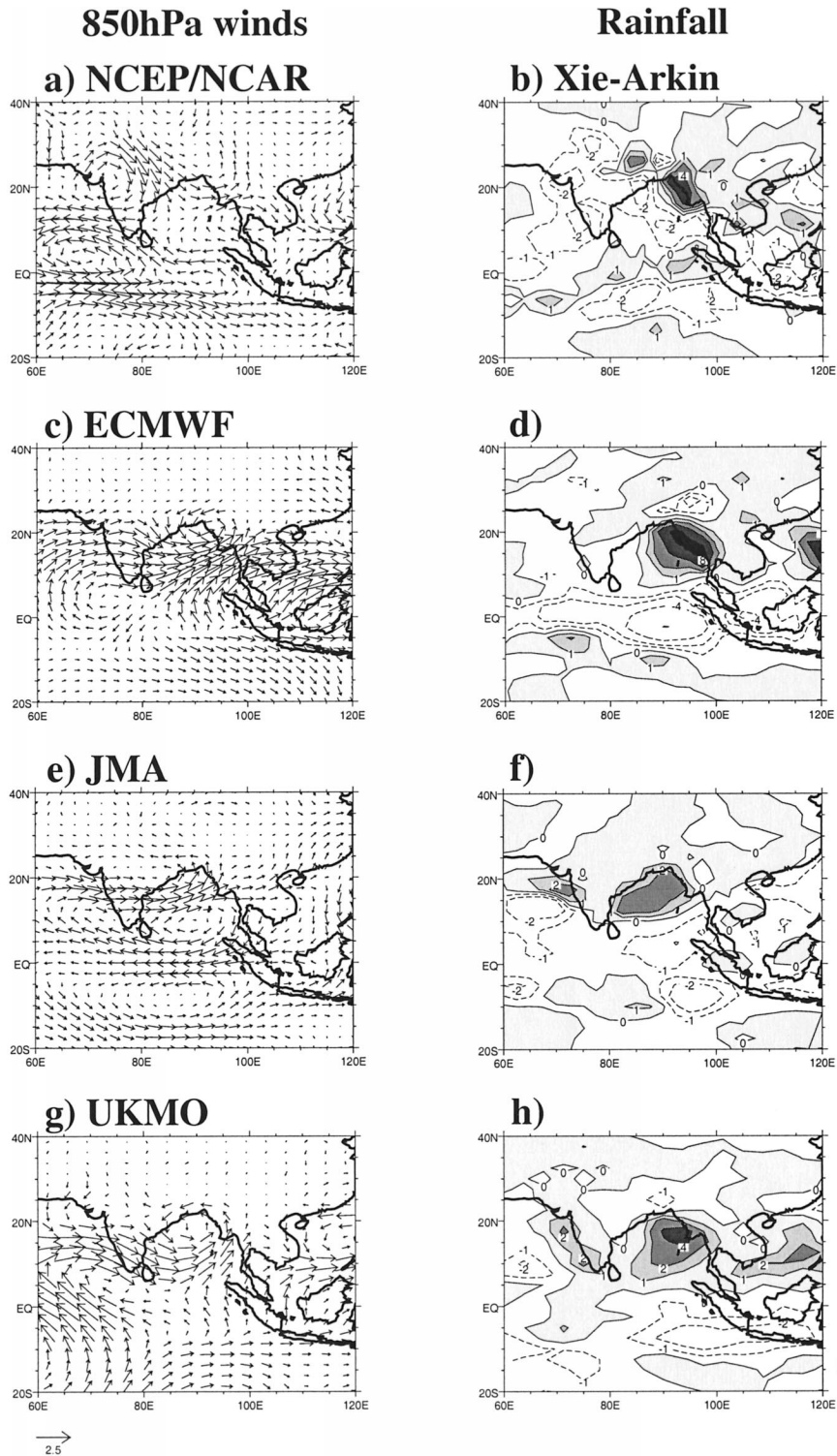


FIG. 10. Jun–Sep averaged 850-hPa wind and rainfall anomalies for 1987 relative to the base period 1987, 1988, and 1993. For the models, the anomalies are calculated with respect to the time mean of all ensemble members. Positive rainfall anomalies are shaded, and the contour interval is $\pm 0, 1, 2, 4, 8, \dots$ mm day $^{-1}$. A unit vector corresponds to 2.5 m s $^{-1}$.

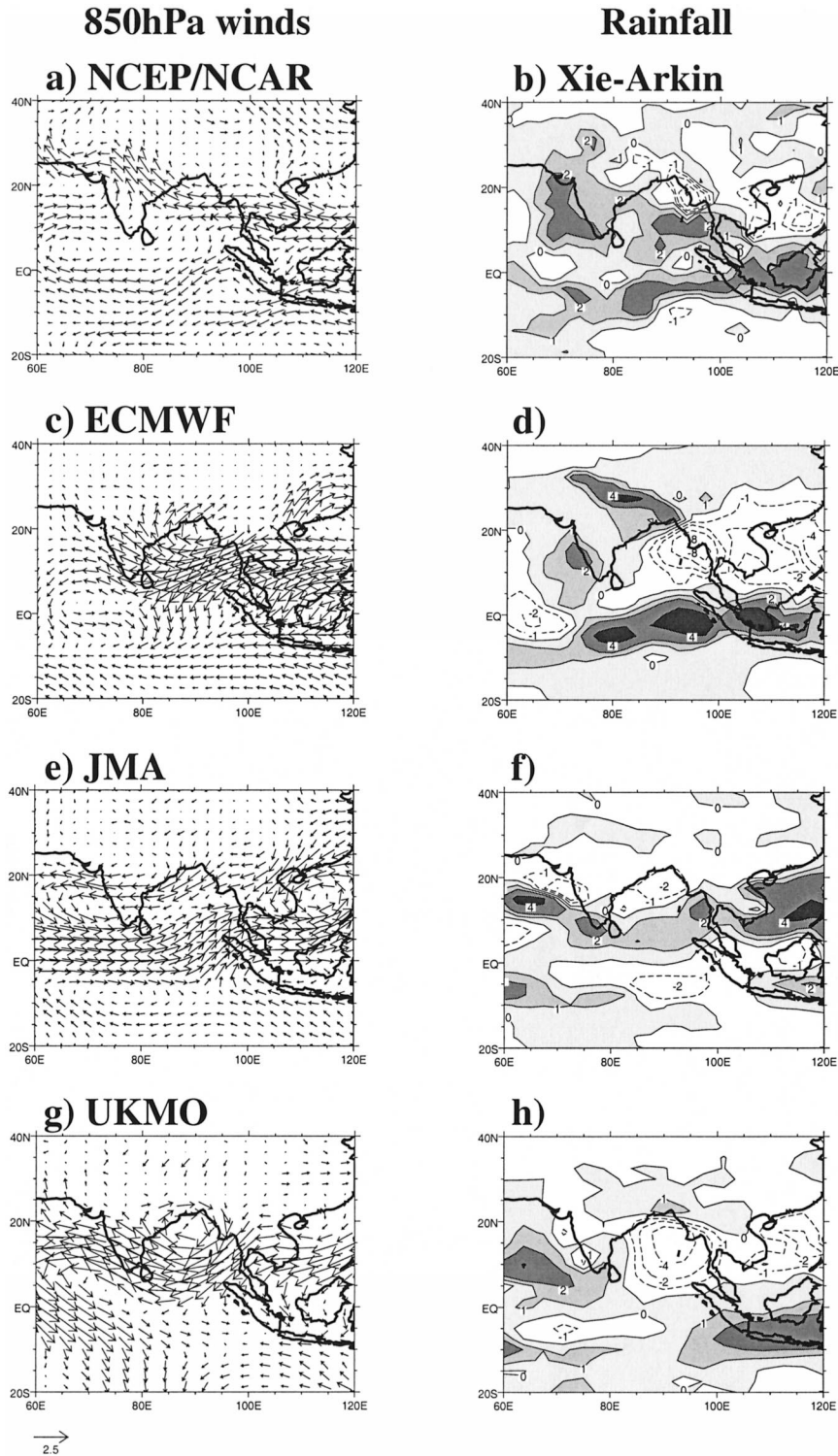


FIG. 11. As in Fig. 10 for 1988.

clonic anomalies near northwest India, and onshore flow near the western Ghats, enhanced rainfall dominates the Indian subcontinent and much of the Bay of Bengal.

The ECMWF model correctly simulates enhanced

rainfall in the vicinity of India and the equatorial Indian Ocean (Fig. 11d). The southeasterly wind anomalies (Fig. 11c) over India are similar to observations, but the simulation lacks the onshore flow along the west coast

of India seen in the reanalysis (Fig. 11a). Table 5 and Fig. 9a indicate that the wind anomalies are strongly dominated by negative loadings of PC-1. Recalling that the rainfall anomalies associated with EOF-1/PC-1 (Fig. 6b) are incorrect over India, the negative loadings of PC-1 incorrectly dominate the signature of enhanced rainfall over India. Thus, this model captures the correct rainfall signal due to the excessive magnitude of PC-1 and its improper subseasonal link to rainfall over India.

As seen in Table 6 for JMA, the projections of PCs-1–3 on the seasonal anomalies are incorrectly simulated (averaged over all ensemble members), consistent with the poor simulation of the wind and rainfall anomalies in 1988 (Figs. 11e,f).

UKMO is similar to ECMWF in that PC-1 incorrectly dominates the projections onto the seasonal anomaly (Table 7). This dominant negative loading gives rise to the southeasterly flow over India (Fig. 11g) and the tendency for negative rainfall anomalies over the Indian subcontinent (Fig. 11h).

d. 1993

The observed loadings indicate PC-1 to be the dominant contributor to the wind anomalies in 1993. As seen in Table 5, ECMWF exhibits mixed signals in 1993, and for some of the realizations higher-order EOFs dominate, unlike the observed projections. Thus, the 850-hPa wind and the rainfall anomalies, given in Figs. 12c,d, are inconsistent with observations.

For JMA, the incorrect negative projections of PC-1 for three of four members (Table 6) are further complicated by strong projections of higher-order modes (not shown), thus resulting in the poor simulation of the 1993 anomalies (Figs. 12e,f).

As seen in Fig. 12g, the UKMO model gives a qualitatively correct representation of the wind anomalies in 1993. This is due to the correct signs of the projections of PCs 1–2 in three of four members, as seen in Table 7. The corresponding rainfall pattern in Fig. 12h contains elements of the observed rainfall pattern, with the tendency for above-normal rainfall over northern India and below-normal rainfall to the south. The above-normal rainfall over northern India is not as coherent as observed since the model locates the cyclonic wind anomalies over the northwestern Bay of Bengal rather than over northern India.

From examination of all seven models we find that the spatial patterns of the dominant subseasonal EOFs are simulated with varying degrees of fidelity (Table 4). The projections of the PCs from the BMRC, CNRM, DNM, and SAWB models are given in Tables 8–11. As with ECMWF, JMA, and UKMO, they are typically poor at representing the projections of the PCs onto the interannual variability.

We have highlighted the EOFs that contribute to errors in the simulation of the seasonal anomalies. Even

though the first EOF/PC is observed to vary randomly, several models exhibit systematic perturbations of the PCs, and they overestimate its influence relative to the other PCs. For 1987 and 1988 all BMRC members captured the proper projections of PC-3 (PC-2 from BMRC, Table 8), but errors in the simulation of the other PCs dominate the seasonal anomalies and result in a poor simulation of the 850-hPa wind anomalies (not shown). From JMA (Table 6), all members had the incorrect sign of the projections of PC-3 in 1987 and 1988, even though this model gave the best representation of EOF-3 (Fig. 5c, Table 4). This highlights the importance of simulating the correct interannual projections of these modes. In the case of the boundary forced modes, such errors indicate that the model is failing to capture observed teleconnections.

PC-2 should have negative loadings in 1987, as anticipated from the results of Sperber et al. (2000a). JMA, BMRC, and CNRM (Tables 6, 8, and 9) captured this feature. For the other models, the incorrect representation of the PC-2 loadings indicates that the models are not properly simulating the El Niño–ASM teleconnection. This may be associated with poorly representing the location, magnitude, and/or vertical profile of the diabatic heating in the tropical Pacific associated with El Niño. Given the importance of simulating the interannual projections of the subseasonal modes, the performance of the ensemble members will be analyzed objectively by stratifying the integrations according to their projections onto the interannual variability.

e. Objective performance of the ensemble members

We have shown that improperly simulating the projections of the EOFs/PCs is associated with a poor representation of the interannual variability. To firmly conclude that subseasonal interactions are important for the interannual variability, we must demonstrate that proper projections result in an improved simulation of the interannual variability. This would also provide the added benefit of being able to objectively discriminate among the performance of the individual ensemble members. However, particularly for rainfall, improvement is intimately linked to a model's ability to represent the observed rainfall perturbations associated with each of the subseasonal EOFs/PCs (Figs. 6–8).

From examination of Tables 5–11, we see that none of the ensemble members were able to properly simulate the correct sign of the observed projections in 1987. However, in 1988 several of the models had at least one realization that was successful in this regard (see bold entries in the tables). For brevity, we confine our remarks to the ECMWF, JMA, and UKMO ensembles. Figures 13a,b show the anomalies from the ECMWF realization that was started with the 28 May 1988 initial conditions. Based on the data in Table 5, this member was chosen since it is not incorrectly dominated by PC-1, whose rainfall signal over India was incorrect

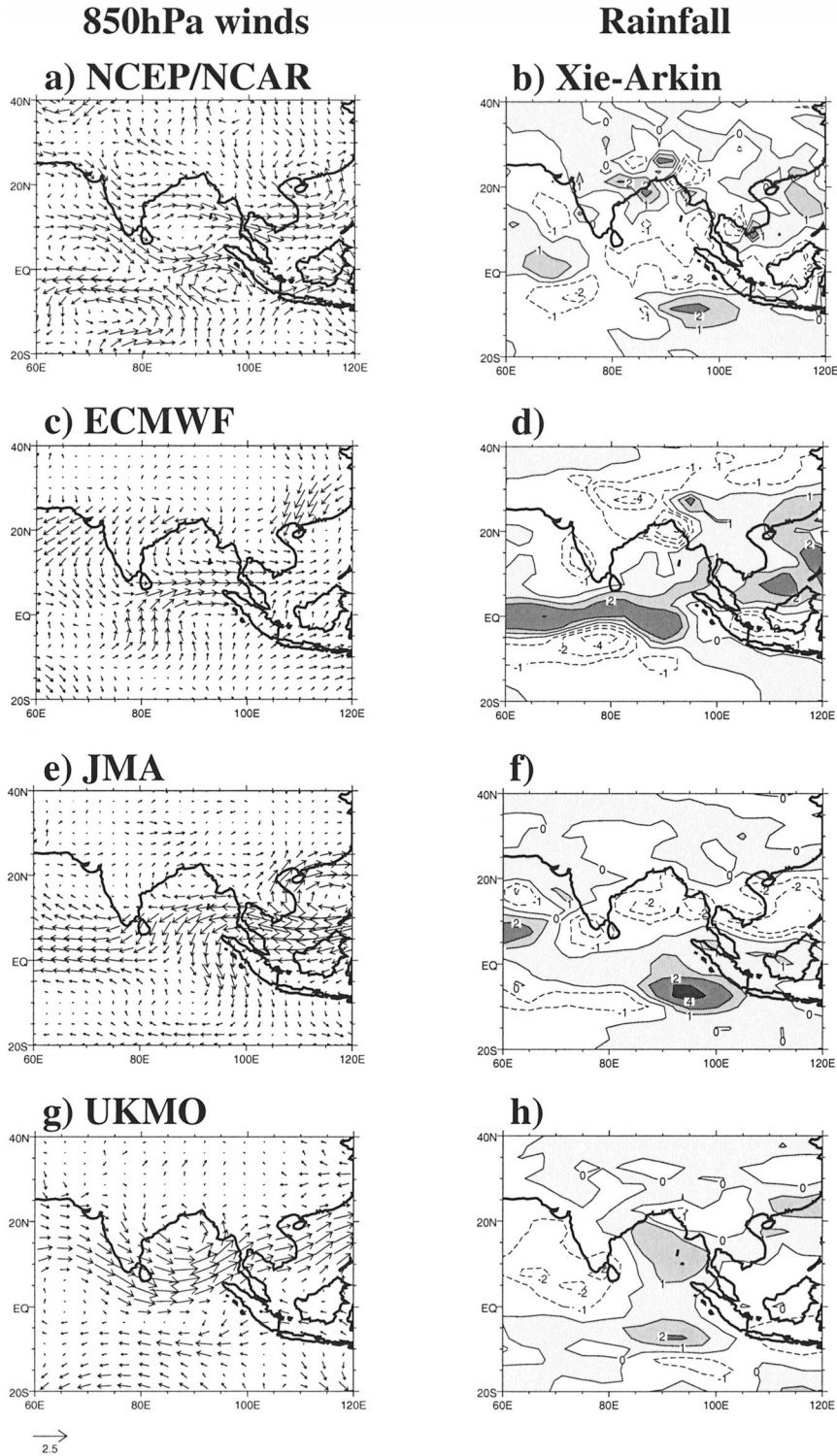


FIG. 12. As in Fig. 10 for 1993.

(Fig. 6b). In Fig. 13a there is an improved representation of the onshore flow adjacent to the west coast of India relative to Fig. 11c, but the southeasterlies in the vicinity of the monsoon trough are now absent. This is because

the EOF-3 cyclone–anticyclone pattern (Fig. 5b) is shifted east of the observed location (Fig. 5a). Hence easterly anomalies are located just to the north of the Bay of Bengal rather than over northern India. This indicates

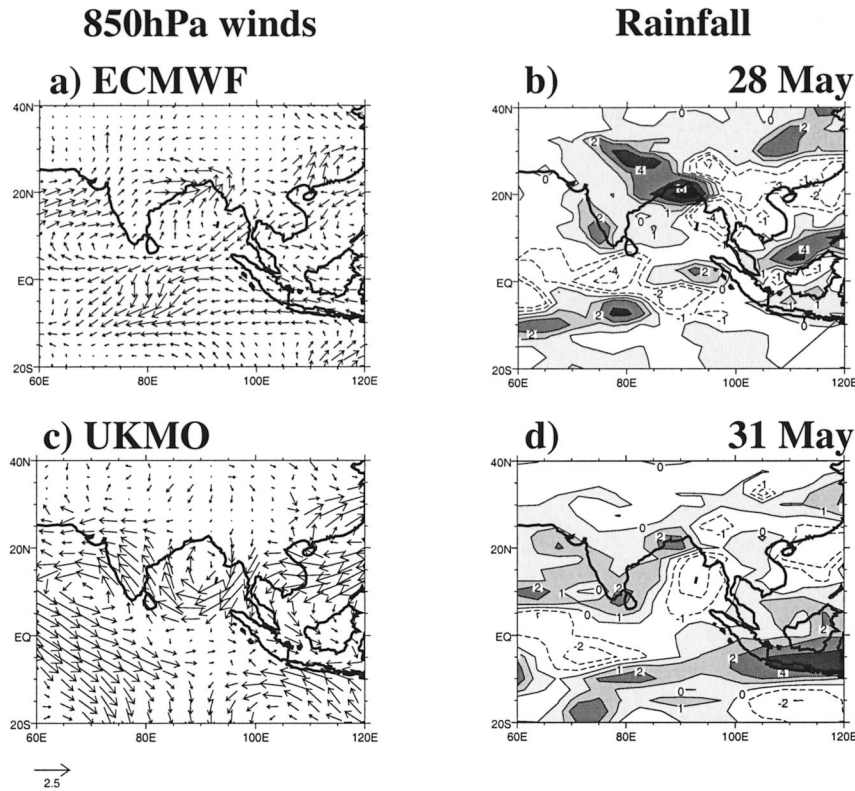


FIG. 13. As in Fig. 10, but for ensemble members in 1988 that had the correct signs of the projections of the PC time series. The date corresponds to the start date of the integration.

that it is important to minimize the spatial errors of each EOF and to properly represent the partitioning of the loadings among the PCs to quantitatively represent the interannual variability.

The 31 May 1988 UKMO simulation shows the most substantial improvement given the correct sign of the loading of PC-6 (PC-3 from reanalysis; Table 7). As seen in Fig. 13c, this member has a more realistic orientation of the flow along the monsoon trough and the cyclonic flow southwest of India relative to Fig. 11g. Additionally, the cyclonic flow at the head of the Bay of Bengal is more realistic (Fig. 13c). Associated with the improved 850-hPa wind anomalies is a more realistic representation of the enhanced rainfall anomalies over India and the below-normal anomalies over the Bay of Bengal (Fig. 13d).

During 1993, the composite wind and rainfall anomalies from the ECMWF 23, 25, and 29–30 May integrations do not show any improvement in the 850-hPa and the rainfall anomalies (Figs. 14a,b), even though the signs of the projections of the PCs agree with the reanalysis (Table 5). Two reasons contribute to this shortfall: 1) as noted earlier, the incorrect sign of the PC-1 composite rainfall anomalies over India (Fig. 6b) and 2) the stronger contributions of higher-order EOFs (not shown).

JMA shows dramatic improvement in its 1 June 1993

simulation, as seen in Figs. 14c,d, due to the positive projection of PC-1 (Table 6). However, the excessively strong positive projection of PC-3 also contributes to the enhanced rainfall in the vicinity of India, which is stronger than observed.

From UKMO, the 30 May 1993 run has easterly anomalies over northern India, slightly south of the observed location, and improved rainfall over the subcontinent.

We have been able to stratify model performance according to the projections of the subseasonal modes onto the interannual variability. In the majority of cases, the 850-hPa wind and the rainfall anomalies were improved for members that simulated correctly the sign of the observed projections. This is especially true for those models that were most realistic at representing the subseasonal link between the 850-hPa flow and the rainfall. The improvement is tempered by the need to also simulate more realistic amplitudes of the observed projections.

6. Discussion and conclusions

We have investigated dynamical seasonal predictability of the Asian summer monsoon using ensembles of hindcasts from seven models forced with observed SSTs and run from observed initial conditions. DSP is

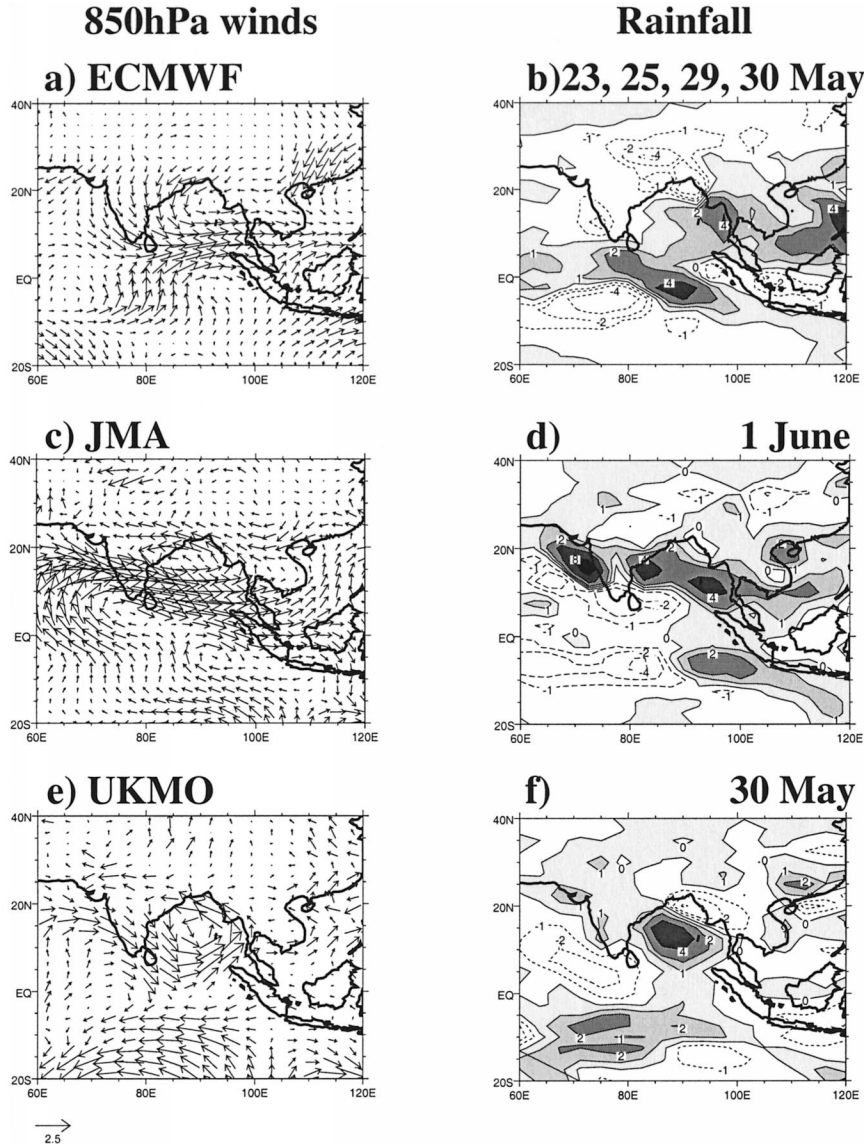


FIG. 14. As in Fig. 13, but for 1993.

addressed by evaluating the link between subseasonal and interannual variability. With respect to the goals of the paper outlined in section 1, first, our results indicate that a high degree of fidelity is required in the simulation of the dominant EOFs of subseasonal variability. Errors in the spatial patterns relative to observations inhibit the simulation of the observed interannual anomalies and are related to errors in the mean state of the model.

Second, the rainfall anomalies associated with the subseasonal EOFs must agree well with the observations in order to have the potential for DSP of rainfall. Errors in the magnitude and spatial patterns of the subseasonal rainfall anomalies are detrimental to DSP since they can result in the incorrect sign of the anomalies on interannual timescales. In this respect the most dramatic example is the simulation of rainfall anomalies of the in-

correct sign over India for EOF-1/PC-1 in the case of ECMWF (Fig. 6b), BMRC, DNM, and SAWB (latter three examples not shown). In these cases, even though a model may properly project this EOF/PC onto the interannual variability, the rainfall signal over India will be of opposite sign relative to the observed projection. Over and above this, even where the sign of the rainfall anomalies agree with observations in Figs. 6–8, the amplitudes can differ substantially, making quantitative assessment of the total seasonal anomaly an extremely challenging problem.

Third, the models usually fail to properly project the subseasonal PCs onto the seasonal mean monsoon with the result of poor DSP of the Asian summer monsoon. In cases where the subseasonal EOFs and their associated rainfall variations are well simulated by a model,

and are known to be linked to aspects of the boundary forcing, projections of the incorrect sign indicate that the model is not generating the necessary teleconnections. A prime example is the JMA model, which gives an excellent representation of the subseasonal EOFs and their associated rainfall patterns (Figs. 3c–9c). In particular, the EOF that is most important for all-India rainfall in observations is best simulated by this model (Fig. 5c, Table 4). However, the interannual variability of this EOF/PC is incorrectly simulated (Table 6 and Fig. 9f), contributing directly to the poor simulation of the 850-hPa wind and rainfall anomalies over India (and the ASM region in general; see Figs. 10e,f and 11e,f). In the case of the El Niño forced mode (EOF-2/PC-2, Sperber et al. 2000a) the poor projections by the models could be related to errors in the location, magnitude, and vertical representation of the ENSO-related diabatic heating.

Fourth, we find that given a reasonable representation of the subseasonal EOFs and their associated rainfall variations, it is found that when an ensemble member can simulate the correct signs of the observed projections these members give a more realistic representation of the observed anomalies. This serves as a method of objectively discriminating among the ensemble members, although only in an a posteriori manner.

More accurate DSP would be achieved if realistic relative loadings of the PCs were captured by the models, but this is presently beyond the scope of the current models. Additionally, as discussed in Sperber et al. (2000a), the simulation of higher-order EOFs is necessary to portray smaller-scale monsoon variations, such as migration of the Mei-yu front. Importantly, this study also sheds light on the subseasonal EOFs that are associated with systematic model error on interannual timescales and in their time mean states. If the underlying physics of these aspects of subseasonal variability can be understood in detail, this would result in improvement of a model's interannual variability.

Additionally, the results in Figs. 3–8 indicate that there may be a sensitivity to horizontal resolution. The two coarsest resolution models, DNM and SAWB (Table 1), have difficulty in representing the subseasonal EOFs (Table 4; see also Sperber et al. 2000b), including the strong gradients and regional-scale features in the 850-hPa flow. This result is consistent with the horizontal resolution study of Sperber et al. (1994), the only resolution study to examine subseasonal variability of the ASM for the range of resolutions in Table 1. They found that T21 was inadequate for simulating the synoptic-scale evolution of the monsoon trough and variations of the Mei-yu rainband over China. Rather, they concluded that a horizontal resolution of T106 ($\sim 1.125^\circ$) was required to simulate these phenomena. Subsequent improvement is indicated by the results presented herein and the results of Martin (1999), who found that $2.5^\circ \times 3.75^\circ$ ($\sim T42$) is adequate for the simulation of intraseasonal variability of the summer monsoon. How-

ever, these aforementioned resolution studies, and those of Tibaldi et al. (1990), Lal et al. (1997), and Stephenson et al. (1998), indicate that increasing horizontal resolution is not the panacea for improving the simulation of summer monsoon variability. Rather, the interaction between physics parameterizations, in particular convection and resolution (both horizontal and vertical), needs to be understood in more detail as part of an overall program to more accurately represent monsoon dynamics.

Acknowledgments. K. R. Sperber would like to thank Dr. Gill Martin (Hadley Centre) for her helpful comments on an earlier draft of this work, Prof. Julia Slingo for helpful discussions, anonymous reviewers for helpful suggestions, and Dr. Mike Fiorino (PCMDI) for assistance in processing ECMWF GRIB data. The NCEP–NCAR Reanalysis was obtained from NOAA CIRES. The pentad CMAP data were provided by Drs. Pingping Xie and Phil Arkin, and the GPCP data were obtained from NOAA NCDC. This work was performed under the auspices of the U.S. Department of Energy by University of California Lawrence Livermore National Laboratory under Contract W-7405-Eng-48.

REFERENCES

- Alekseev, V. A., E. M. Volodin, V. Galin, V. P. Dymnikov, and V. N. Lykossov, 1999: Modeling of the present-day climate by the atmospheric model of INM RAS "DNM GCM." Description of the model version A5421 and results of AMIP II simulations. INM Rep. N2086-B98, 208 pp. [Available from Institute for Numerical Mathematics, Gubkina 8, Moscow 117951 GSP-1, Russia.]
- Annamalai, H., J. M. Slingo, K. R. Sperber, and K. Hodges, 1999: The mean evolution and variability of the Asian summer monsoon: Comparison of ECMWF and NCEP/NCAR reanalyses. *Mon. Wea. Rev.*, **127**, 1157–1186.
- Barnett, T. P., L. Dumenil, U. Schlese, E. Roeckner, and M. Latif, 1989: The effect of Eurasian snow cover on regional and global climate variations. *J. Atmos. Sci.*, **46**, 661–685.
- Becker, B. D., J. M. Slingo, L. Ferranti, and F. Molteni, 2001: Seasonal predictability of the Indian summer monsoon: What role do land surface conditions play? *Mausam*, in press.
- Blanford, H. F., 1884: On the connection of the Himalaya snowfall with dry winds and seasons of drought in India. *Proc. Roy. Soc. London*, **37**, 3–22.
- Brankovic, C., and T. N. Palmer, 2000: Seasonal skill and predictability of ECMWF PROVOST ensembles. *Quart. J. Roy. Meteor. Soc.*, **126**, 2035–2067.
- Charney, J. G., and J. Shukla, 1981: Predictability of monsoons. *Monsoon Dynamics*, Sir J. Lighthill and R. P. Pearce, Eds., Cambridge University Press, 99–110.
- Déqué, M., and J. P. Piedelievre, 1995: High resolution climate simulation over Europe. *Climate Dyn.*, **11**, 321–339.
- Fennessy, M. J., and J. Shukla, 1994: GCM simulations of active and break monsoon periods. *Proc. Int. Conf. on Monsoon Variability and Prediction*, Vol. 2, Trieste, Italy, WCRP-84, WMO/TD-No. 619, 576–585.
- Ferranti, L., and F. Molteni, 1999: Ensemble simulations of Eurasian snow-depth anomalies and their influence on the summer Asian monsoon. *Quart. J. Roy. Meteor. Soc.*, **125**, 2597–2610.
- , J. M. Slingo, T. N. Palmer, and B. J. Hoskins, 1997: Relations between interannual and intraseasonal monsoon variability as

- diagnosed from AMIP integrations. *Quart. J. Roy. Meteor. Soc.*, **123**, 1323–1357.
- Gadgil, S., and G. Asha, 1992: Intraseasonal variation of the summer monsoon I: Observational aspects. *J. Meteor. Soc. Japan*, **70**, 517–527.
- Gibson, J. K., P. Kallberg, and S. Uppala, 1996: The ECMWF ReAnalysis (ERA) project. *ECMWF Newsl.*, **73**, 7–17.
- , —, —, A. Hernandez, A. Nomura, and E. Serano, 1997: ECMWF ReAnalysis Project Rep. Series 1, ECMWF, Shinfield Park, Reading, United Kingdom, 72 pp.
- Graham, R. J., A. D. L. Evans, K. R. Mylne, M. S. J. Harrison, and K. B. Robertson, 2000: An assessment of seasonal predictability using atmospheric general circulation models. *Quart. J. Roy. Meteor. Soc.*, **126**, 2211–2240.
- Gruber, A., X. Su, M. Kanamitsu, and J. Schemm, 2000: The comparison of two merged rain-gauge-satellite precipitation datasets. *Bull. Amer. Meteor. Soc.*, **81**, 2631–2644.
- Hall, C. D., R. A. Stratton, and M. L. Gallani, 1995: Climate simulations with the Unified Model: AMIP runs. Met Office Climate Research Tech. Note 61, 94 pp. [Available from National Meteorological Library, London Road, Bracknell, Berkshire RG12 2SZ, United Kingdom.]
- Hart, T. L., W. Bourke, B. J. McAvaney, B. W. Forgan, and J. L. McGregor, 1990: Atmospheric general circulation simulations with the BMRC global spectral model: The impact of revised physical parameterizations. *J. Climate*, **3**, 436–459.
- Huffman, G. J., R. F. Adler, B. Rudolf, U. Schneider, and P. R. Keehn, 1995: Global precipitation estimates based on a technique for combining satellite-based estimates, rain gauge analysis, and NWP model precipitation information. *J. Climate*, **8**, 1284–1295.
- , and Coauthors, 1997: The Global Precipitation Climatology Project (GPCP) combined precipitation dataset. *Bull. Amer. Meteor. Soc.*, **78**, 5–20.
- JMA, 1997: Outline of operational numerical weather prediction at the Japan Meteorological Agency. Numerical Prediction Division, Japan Meteorological Agency, Tokyo, Japan, 126 pp.
- Kalnay, E., and Coauthors, 1996: The NCEP/NCAR 40-Year Reanalysis Project. *Bull. Amer. Meteor. Soc.*, **77**, 437–471.
- Kirtman, B. P., J. Shukla, B. Huang, Z. Zhu, and E. K. Schneider, 1997: Multiseasonal predictions with a coupled tropical ocean–global atmosphere system. *Mon. Wea. Rev.*, **125**, 789–808.
- Krishna Kumar, K., M. K. Soman, and K. Rupa Kumar, 1995: Seasonal forecasting of Indian summer monsoon rainfall. *Weather*, **50**, 449–467.
- Krishnamurthy, V., and J. Shukla, 2000: Intraseasonal and interannual variability of rainfall over India. *J. Climate*, **13**, 4366–4377.
- Krishnamurti, T. N., and H. N. Bhalme, 1976: Oscillations of a monsoon system. Part I. Observational aspects. *J. Atmos. Sci.*, **33**, 1937–1954.
- Lal, M., U. Cubasch, J. Perlwitz, and J. Waszkewitz, 1997: Simulation of the Indian monsoon climatology in ECHAM3 climate model: Sensitivity to horizontal resolution. *Int. J. Climatol.*, **17**, 847–858.
- Martin, G., 1999: The simulation of the Asian summer monsoon, and its sensitivity to horizontal resolution, in the UK Meteorological Office Unified Model. *Quart. J. Roy. Meteor. Soc.*, **125**, 1499–1525.
- McAvaney, B. J., and R. A. Colman, 1993: The AMIP experiment: The BMRC AGCM configuration. BMRC Research Rep. 38, Bureau of Meteorology, 43 pp.
- Miller, M., M. Hortal, and C. Jakob, 1995: A major operational forecast model change. *ECMWF Newsl.*, **70**, 2–5.
- Mo, K. C., and R. W. Higgins, 1996: Large-scale atmospheric moisture transport as evaluated in the NCEP/NCAR and the NASA/DAO reanalyses. *J. Climate*, **9**, 1531–1545.
- Normand, C., 1953: Monsoon seasonal forecasting. *Quart. J. Roy. Meteor. Soc.*, **79**, 463–473.
- Palmer, T. N., 1994: Chaos and predictability in forecasting the monsoon. *Proc. Indian Natl. Sci. Acad.*, **60A**, 57–66.
- Pan, H. L., and L. Mahrt, 1987: Interaction between soil hydrology and boundary layer developments. *Bound.-Layer Meteor.*, **38**, 185–202.
- , and W. S. Wu, 1994: Implementing a mass-flux convection parameterization package for the NMC medium-range forecast model. Preprints, *10th Conf. on Numerical Weather Prediction*, Portland, OR, Amer. Meteor. Soc., 96–98.
- Sikka, D. R., 1980: Some aspects of the large-scale fluctuations of summer monsoon rainfall over India in relation to fluctuations in the planetary and regional scale circulation parameters. *Proc. Indian Acad. Sci. (Earth and Planet. Sci.)*, **89**, 179–195.
- Slingo, J. M., 1987: The development and verification of a cloud prediction scheme for the ECMWF model. *Quart. J. Roy. Meteor. Soc.*, **113**, 899–927.
- Sperber, K. R., and T. N. Palmer, 1996: Interannual tropical rainfall variability in general circulation model simulations associated with the Atmospheric Model Intercomparison Project. *J. Climate*, **9**, 2727–2750.
- , S. Hameed, G. L. Potter, and J. S. Boyle, 1994: Simulation of the northern summer monsoon in the ECMWF model: Sensitivity to horizontal resolution. *Mon. Wea. Rev.*, **122**, 2461–2481.
- , J. M. Slingo, and H. Annamalai, 1999: Predictability and the relationship between subseasonal and interannual variability during the Asian summer monsoon. PCMDI Rep. 53, 53 pp. [Available from Lawrence Livermore National Laboratory, P.O. Box 808, L-264, Livermore, CA 94550; also online at <http://www-pcmdi.llnl.gov/pcmdi/pubs/ab53.html>.]
- , —, and —, 2000a: Predictability and the relationship between subseasonal and interannual variability during the Asian summer monsoon. *Quart. J. Roy. Meteor. Soc.*, **126**, 2545–2574.
- , and Coauthors, 2000b: Dynamical seasonal predictability of the Asian summer monsoon. PCMDI Rep. 56, 56 pp. [Available from Lawrence Livermore National Laboratory, P.O. Box 808, L-264, Livermore, CA 94550; also online at <http://www-pcmdi.llnl.gov/pcmdi/pubs/ab56.html>.]
- Stendel, M., and K. Arpe, 1997: Evaluation of the hydrological cycle in reanalyses and observations. Max-Planck-Institut für Meteorologie, Hamburg, Germany, Rep. 228, 52 pp.
- Stephenson, D. B., F. Chauvin, and J.-F. Royer, 1998: Simulation of the Asian summer monsoon and its dependence on model horizontal resolution. *J. Meteor. Soc. Japan*, **76**, 237–265.
- Tennant, W. J., 1999: The potential for the numerical forecasting of monthly climate over South Africa. *Int. J. Climatol.*, **19**, 1319–1336.
- Tibaldi, S., T. N. Palmer, C. Brankovic, and U. Cubasch, 1990: Extended-range predictions with ECMWF models: Influence of horizontal resolution on systematic error and forecast skill. *Quart. J. Roy. Meteor. Soc.*, **116**, 835–866.
- Tiedtke, M., 1989: A comprehensive mass flux scheme for cumulus parameterization. *Mon. Wea. Rev.*, **117**, 1779–1800.
- , 1993: Representation of clouds in large-scale models. *Mon. Wea. Rev.*, **121**, 3040–3061.
- Viterbo, P., and A. C. M. Beljaars, 1995: An improved land surface parameterization scheme in the ECMWF model and its validation. *J. Climate*, **8**, 2716–2748.
- Walker, G. T., and E. W. Bliss, 1930: Some applications to seasonal foreshadowing. *Mem. Roy. Meteor. Soc.*, **3**, 81–95.
- Webster, P. J., and S. Yang, 1992: Monsoon and ENSO: Selectively interactive systems. *Quart. J. Roy. Meteor. Soc.*, **118**, 877–926.
- , T. N. Palmer, M. Yanai, J. Shukla, V. Magnana, T. Yasunari, and R. Tomas, 1998: The monsoon: Processes, predictability and prediction. *J. Geophys. Res.*, **103**, 14 451–14 510.
- Xie, P., and P. Arkin, 1996: Analyses of global monthly precipitation using gauge observations, satellite estimates, and numerical model predictions. *J. Climate*, **9**, 840–858.
- , and —, 1997: Global precipitation: A 17-year monthly analysis based on gauge observations, satellite estimates, and numerical model outputs. *Bull. Amer. Meteor. Soc.*, **78**, 2539–2558.